Acta Mech. Sin. (2017) 33(4):685–708
DOI 10.1007/s10409-017-0685-4

REVIEW PAPER

Dynamics of cavitation–structure interaction

Guoyu Wang[1] · **Qin Wu**[1,2] · **Biao Huang**[1]

Received: 19 February 2017 / Revised: 21 April 2017 / Accepted: 3 May 2017 / Published online: 26 June 2017

Abstract Cavitation–structure interaction has become one of the major issues for most engineering applications. The present work reviews recent progress made toward developing experimental and numerical investigation for unsteady turbulent cavitating flow and cavitation–structure interaction. The goal of our overall efforts is to (1) summarize the progress made in the experimental and numerical modeling and approaches for unsteady cavitating flow and cavitation–structure interaction, (2) discuss the global multiphase structures for different cavitation regimes, with special emphasis on the unsteady development of cloud cavitation and corresponding cavitating flow-induced vibrations, with a high-speed visualization system and a structural vibration measurement system, as well as a simultaneous sampling system, (3) improve the understanding of the hydroelastic response in cavitating flows via combined physical and numerical analysis, with particular emphasis on the interaction between unsteady cavitation development and structural deformations. Issues including unsteady cavitating flow structures and cavitation–structure interaction mechanism are discussed.

Keywords Cavitation–structure interaction · Unsteady cavitating flows · Cavitating flow-induced vibration · Hydroelastic response

✉ Guoyu Wang
wangguoyu@bit.edu.cn

[1] School of Mechanical Engineering, Beijing Institute of Technology, Beijing 100081, China

[2] Department of Thermal Engineering, Tsinghua University, Beijing 100084, China

List of symbols

σ	Local cavitation number
C_{dest}, C_{prod}	Constant rate for vaporization and condensation
C_h	Bending damping coefficient
C_θ	Torsional damping coefficient
C_l	Lift coefficient
C_d	Drag coefficient
C_m	Moment coefficient
c	Chord length of hydrofoil
Cp	Pressure coefficient
D	Drag
f	Frequency
h	Bending deformation
I_θ	Moment of inertia
K_h, K_θ	Structural stiffness values for bending and twisting motion
k	Turbulent kinetic energy
L	Cavity length
L_{ref}	Reference length
L_f	Lift
M	Moment
m	mass of structure
m^+, m^-	Source and sink terms in the cavitation model
p	Pressure
p_∞	Reference static pressure
R	Bubble diameter
Re	Reynolds number
S_θ	Static imbalance
Fr	Froude number
s	Span of hydrofoil
t	Local time

t_∞	Reference time scale, $t_\infty = L/U_\infty$
T_{ref}	Reference periodic time
U_∞	Reference velocity
$V_{\text{v},n}$	Normal component of the vapor velocity moving away from the interface
$V_{\text{I},n}$	Normal interfacial velocity
ωz	z-component of the vorticity
x	Space variable
δy	Maximum of vibration amplitude
α	Angle of attack
α_{l}	Liquid volume fraction
α_{v}	Vapor mass fraction
ρ	Density
θ	Twist deformation
μ	Dynamic viscosity
$\mu_T/\mu_{\text{L}\vert\text{inlet}}$	Eddy-to-laminar viscosity ratio at the inlet
ε	Turbulent dissipation rate
λ	Filter size in filter-based model

Subscript

i, j	Component
l	Liquid
v	Vapor
L	Laminar
m	Mixture property
T	Turbulent

1 Introduction

Cavitation occurs when the local pressure drops below the saturated vapor pressure and may lead to the formation of vaporous bubble(s), which is a complex, unsteady, multiscale, and multiphase flow phenomenon [1,2]. Cavitation is related to the key technical problems in a wide range of engineering applications, such as fluid machinery, thermal power generation, as well as underwater weapons, since the occurrence of cavitation can lead to problems, including pressure pulsations, sudden changes in loads, vibrations, noise, and erosion [3–5]. So, it is of primary importance to predict accurately the unsteady cavitation evolution, and the resultant impact on the system performance. With the increasing demand of higher performance and efficiencies for marine propulsion and hydropower system, structures became more flexible and were subjected to high flow rates. The fluid–structure interaction (FSI) has become one of the major issues in a large variety of applications, which will produce stronger structural vibrations with more complex flow-excitation mechanisms. Especially when cavitation occurs, accompanied by complex interaction between phase-change and vortex structures. The transient loads induced by the unsteady breakdown and shedding of the cavities will further lead to hydrodynamic instabilities and even structure failures in a relatively short time, which may become the major issue for the safe and stable system operation. In order to address the critical technical issue related to the marine propulsion and engineering problems, the unsteady cavitation and cavitation–structure interaction has been investigated via combined physical and numerical studies.

1.1 Key aspects in unsteady cavitation structures and dynamics

Review of the literature regarding the geometry, unsteadiness, turbulence, and flow structure interplay in experimental study is summarized to help understand cavitation phenomenon, and also to compare with the simulation results as code validations.

1.1.1 Experimental methods

With the decrease of local fluid pressure, the cavity structure changes from inception cavitation with localized, instantaneous pressure drop, to sheet, cloud, and supercavitation with time-dependent cavities observed [6–9]. The highly turbulent and unsteady cavitation have been investigated experimentally by many researchers.

In their work, Kubota et al. [10] have investigated a stationary hydrofoil in steady inlet flow and demonstrated the unsteady cloud cavitation structures. To investigate further cloud cavitation, Kawanami et al. [7] have demonstrated that the re-entrant jet is rushed from the rear end of the cavity to the leading edge where it triggers cloud cavity shedding. The cavitation instability induced by the development of a re-entrant jet is also studied with the case of flow past a backstep channel [11]. According to the origin of the unsteadiness, intrinsic instability and system instability are the two main classes of instabilities, among which the re-entrant jet mechanism is an intrinsic instability, while the system instability originates from the interaction between the cavity and the rest of the system [12].

Various experimental techniques have been developed to study the complex multiphase flow structures.

The work by Kubota et al. [10] used laser Doppler velocimetry (LDV) to measure the flow velocity around cloud cavitation. It was found that the mean velocity in the cloud cavity was lower than the mean stream velocity and an increase in vorticity was measured. LDV has been applied successfully for cavitating flows, but cannot yield time-resolved measurements of the velocity field. The study by Li and Ceccio [13] showed that traveling bubbles near the surface leads to local turbulence and also streamwise vorticity. The shedding process of a large-scale cavity has been the focus for a long time, and Arndt and Song [14] conducted

measurements in the wake flow of an NACA 0015 hydrofoil under both cavitation and non-cavitation conditions. They found that the self-similarity of the wake shape existed at the trailing edge.

The study by Li et al. [15] used a particle image velocimetry (PIV) to investigate the developed cavitating flow structures and measure the transient velocity and vorticity. They have shown that in the cavitation region, strong momentum transfer results in a highly even-distributed velocity in the core region of cavitating flow field. Furthermore, Ausoni et al. [16] also applied PIV to study the effect of cavitation on the vortex generation mechanism at the trailing edge of a hydrofoil at Reynolds number $Re = 2.5 \times 10^4 - 6.5 \times 10^4$. The results demonstrated that the transverse velocity near the trailing edge increases the vortex strength linearly, and cavitation in the vortex street cannot be considered a passive agent for the turbulent wake flow.

In their study, Gopalan and Katz [17] applied high-speed photography to measure the sheet cavitation flow structure and demonstrated that the sheet cavity collapse is the main source of vorticity production. In addition, the size change of the cavity results in the change of turbulence level and momentum thickness of the boundary layer.

Geometry together with turbulence, unsteadiness and also 3D effect makes the simulation of cavitation has been a challenging issue for a long time. The work by Laberteaux and Ceccio [8] examined spanwise variation of flow around a hydrofoil. The results showed that the re-entrant jet in the closure region of a 3D partial cavity was redirected away from the cavity interface with a steady cavity attached. Furthermore, Dang and Kuiper [18] studied the re-entrant jet on a hydrofoil with a spanwise varying angle of attack and found that the cavity topology strongly influenced the re-entrant jet direction, which was determined by spanwise distribution of the loading and not by the sweep angle [19]. The study by, Foeth [20] and Foeth et al. [21] observed the collapse of an attached cavity on a 3D hydrofoil and demonstrated that the re-entrant flow from both sides depends on the cavity shape and dictates the behavior of the shedding cycle.

In this section, we have learned that: (1) cavitation is essentially unsteady with turbulence interplay; (2) the re-entrant jet, which comes from the large adverse pressure gradient, will shear the attached cavity into several regions, and the detached cavity will shed downstream, inducing and enhancing the unsteadiness. As a result, if the cavitation model lacks the ability to exhibit transport essence or too much eddy viscosity is modeled from the turbulence closure, it will be very hard to simulate the unsteadiness resulted from re-entrant jet. Moreover, if the pressure and density relation is not given properly in the cavitation model, it cannot accurately predict the dynamics of cavitating flows.

1.1.2 Numerical modeling

Phenomenologically, cavitation is a complex, multi-scale, multiphase phenomenon, and the physical mechanisms have not been fully understood because the complex interaction between turbulent flow structures and phase-change dynamics with large variations in fluid density and pressure fluctuations [22–24]. Hence, there are significant challenges for the computationally simulation of cavitating flow, such as the accuracy, stability, and efficiency of those numerical methods.

1.1.2.1 Cavitation models As for the numerical modeling of cavitation, the selection of cavitation models plays a major role on the prediction of the cavitation development. Recently, significant efforts have been made, and examples of recent review articles can be found in Refs. [25–30]. An overview of a previous cavitation model study is given in Table 1.

The study by Chen and Heister [31], Delannoy and Kueny [35] applied either a barotropic state equation or a transport equation to solve the mixture density field in the homogenous and isothermal multiphase flow. In this way, density is directly coupled with pressure and the iterated enthalpy can determine if the substance is in vapor, liquid, or mixture phase so that each phase can have its own state equation.

In their work, Wang and Ostaoja-Starzewski [36] have developed a single fluid model for modeling the sheet/cloud cavitation. They adopted a fifth-order polynomial curve for different phases to describe the relationship between density coefficient ratio and pressure coefficient when cavitation occurs.

However, these approaches didn't capture some fundamental physical mechanism such as baroclinic vorticity production because the pressure and density gradients are not parallel in fact [17].

The other popular approach to simulate cavitating flows is the transport equation models. An additional transport equation for the mass/volume fraction of vapor is solved, with different source/sink terms be proposed to regulate the mass transfer, which are presented in Refs. [32–34,37].

The study by Kubota et al. [32] solved the local void fraction via the Rayleigh–Plesset equation based on the assumed bubble radius. The results showed that it is appropriate for modeling the unsteady cavitation.

Then, Merkle et al. [37] and Kunz et al. [33] introduced the artificial compressibility method with a pre-conditioning formulation to solve the multiphase unsteady Reynolds-averaged Navier–Stokes (URANS) equations.

The work by Singhal et al. [34] developed a "full cavitation model" derived from a reduced form of the Rayleigh–Plesset equation for bubble dynamics, with the advantage of convective characteristics.

Table 1 Summary of previous cavitation models for simulation of cavitating flows

References	Method (analytic/numerical)	Conclusions (analytic/numerical)
Delannoy and Kueny [31]	Artificial compressibility 2D Navier–Stokes (N–S) equations Density and pressure are coupled by the state/baroclinic equations	Lack of the ability to perform the convection/transport phenomenon and other cavitation behavior
Kubota et al. [32]	Artificial compressibility 2D/3D N–S equations No turbulence model Transport equation model (volume fraction)	Displayed the cloud cavitation mechanism Better to express the generation of such vortex cavitation and the effect of cavitation nuclei in the uniform flow
Kunz et al. [33]	Preconditioning strategy Artificial compressibility 3D N–S equations $k-\varepsilon$ turbulence model Transport equation model (volume fraction)	Agreed well with the experimental result The compressible treatment could improve the dynamics description
Singhal et al. [34]	Incompressibility 2D N–S equations $k-\varepsilon$ turbulence model Transport equation model (mass fraction)	The accuracy of the model and the numerical results are well agreed with experiment data
Senocak and Shyy [26,27]	Incompressibility 2D N–S equations $k-\varepsilon$ turbulence model Transport equation model (volume fraction)	Empirical constants can be replaced by the explicit calculations based on the interfacial dynamics

In order to consider the varying mixture density in the transport process, Senocak and Shyy [25–27] compared different transport equation-based models (TEMs) and developed an interfacial dynamics-based model (IDM), which directly account for the empirical parameters in the current TEMs. Consequently, the density and pressure gradients are not necessarily parallel, so that it can accommodate baroclinic vorticity generation well.

1.1.2.2 Turbulence models Besides cavitation modeling, the turbulence model can significantly influence the cavitating flow structures. An overview of previous turbulent closure study is given in Table 2. As most URANS turbulence models were initially developed for single phase, fully incompressible flows, it is not suitable for compressible, multiphase flow, such as cavitation.

The studies by Reboud et al. [41] and Coutier-Delgosha et al. [38] considered the large density variation in cavitating flow and modified the turbulence eddy viscosity of $k-\varepsilon$ re-normalization group (RNG) model to simulate unsteady cloud cavitation in a Venturi-type duct. The results showed that the modified model better capture the unsteady re-entrant jet and the cloud cavity shedding. However, for those with high cavitation numbers, it cannot predict the cavity length and shedding frequency very well.

Recently, to capture the unsteady characteristics between turbulent small-scale and quasi-periodic large-scale features of the flow field, an LES model was used to simulate sheet/cloud cavitation on a NACA0015 hydrofoil [36]. However, it is fundamentally difficult to find a grid-independent LES solution without a filter scale. Moreover, the computational cost of LES is very high. Very large eddy simulation (VLES) attempts to strike a compromise between RANS and LES. The DES has been widely used as a modified hybrid RANS-LES approach [39]. The study by Huang et al. [42] evaluated an enhanced turbulence modeling scheme based on DES; the results showed that a standard URANS model degraded the ability to predict marginal stable cavities, whereas the DES model appeared to yield more accurate flow modeling, possibly because DES is able to handle the large-scale closure dynamics better.

The work by Johansen et al. [43] proposed an FBM as an accommodation between RANS and LES. Then Wu et al. [40] assessed the validity of FBM turbulence model through the simulation of unsteady flow around various geometries, such as square cylinders, convergent–divergent nozzles, hydrofoils, and so on. The results showed that the FBM model is able to better capture the unsteady features of cavitating flows.

Table 2 Summary of previous turbulence closure models for simulation of cavitating flows

References	Model (analytic/numerical)	Conclusions
Coutier-Delgosha et al. [38]	RANS ($k-\varepsilon$, RNG), with a modified turbulent viscosity, 2D hydrofoil, baroclinic state law, artificial Compressibility	Compressibility effects on two-phase flows are important. Successfully simulated the unsteady self-oscillatory behavior of cavitation
Wang and Ostoja-Starzewski [36]	Large eddy simulation (LES), 3D hydrofoil, baroclinic state law, weakly compressible flows	Successfully simulated unsteady interaction between vortices/bubbles and cavitation structures
Kinzel et al. [39]	Detached eddy simulation (DES), 3D blunt ogive, mixture transport model, compressible flows	DES yield better comparisons with experimental researches than RANS for highly unsteady cavitating flows
Wu et al. [40]	Filter-based model (FBM), 2D divergent nozzle and hydrofoil, mixture transport model, incompressible flows	FBM yielded stronger time-dependency in cavitating flows
Kim and Brewton [28]	RANS, LES, and RANS/LES model, 2D and 3D hydrofoil, mixture transport model, incompressible flows	The LES and the RANS/LES hybrid results can reproduce the salient features of the unsteady sheet/cloud cavitation

The study by Kim and Brewton [28] compared the numerical simulation of sheet/cloud cavitation via RANS, LES, and hybrid RANS/LES approaches. They found that the LES and hybrid approach can reproduce the salient features, such as the formation and the breakup of the cavity, and the collapse of the cloud cavity, accurately.

1.2 Key aspects in cavitation–structure interactions

As mentioned in the above research, temporal periodicity may occur as a result of the cavitating vortex shedding during the cloud cavitation stage, thus leading to many problems, e.g. pressure pulsation, vibration, noise, and erosion, and becoming a primary concern for many engineering problems [44–49]. The work by Kubota et al. [32] measured the unsteady cavitating flow velocity and the pressure fluctuation. They considered that the high frequency component of pressure fluctuation is caused by the impact pressure due to the cavity collapse and the turbulence due to unsteady vortices, while the low frequency component is related to the development and convection of large-scale cloud cavities. Also, Ji et al. [50] analyzed the unsteady cavitating turbulent flow patterns around a three-dimensional twisted hydrofoil and showed that the cavity volumetric acceleration is the main source of the excited pressure fluctuations by cavitation. The study by Chen et al. [51] investigated the cavitation-excited pressure fluctuation in a convergent–divergent channel. They found that the pressure fluctuation was closely related to the time evolution of the cavitation behaviors.

The strong pressure fluctuation can lead to fluctuating hydrodynamic loads which will force on the structure. Hence researchers have paid more and more attention to the presence of the cavitating flow-induced vibrations. The work by De La Torre et al. [52] measured the natural frequencies a hydrofoil under different cavitation condition to investigate the added mass effect on the fluid–structure system. They found that the maximum added mass effect occurs with still water and the minimum with supercavitation.

Recent development of the numerical technique has resulted in noticeable efforts made to use numerical simulation tools. The study by Amromin and Kovinskaya [53] analyzed the vibration of an elastic wing with an attached cavity in periodically perturbed flow by means of the beam equation. This equation showed that cavitation enhances the structural vibration significantly, where the high-frequency band is associated with elastic resonance and the low-frequency band is related to the cavity volume oscillations. Also, Kamakoti and Shyy [54] predicted the flutter performance of an AGARD 445.6 wing at different Mach numbers and showed the capability of the numerical method, which is couples with a complex flow solver, a linear structure solver, as well as moving grid technique. The work by Benaouicha et al. [55] studied the dynamics of a flexible hydrofoil immersed in an unsteady partial cavitating flow based on a weak FSI coupling algorithm. They numerically predicted the forced vibration, which is caused by the periodical partial cavitation, and revealed that the cavitation affects the modal response of flexible structure in a complex interaction process.

An overview of previous fluid–structure interaction model study, which considers the solution of both the fluid and structure domain and the interaction between them, is given in Table 3. The fluid structure interaction algorithms can be generally divided into two categories: monolithic method and partitioned methods. In the monolithic method, the fluid and structure equations are solved simultaneously, but the multi-field problem makes it difficult to implement in many

Table 3 Summary of previous fluid–structure models

References	Model (analytic/numerical)	Conclusions
Ryzhakov et al. [56]	Fully coupled (FC) with flexible structures and free-surface flow	Robust method dealing with FSI problems involving arbitrary variations in the shape of the fluid domain
		Completed free of spurious added-mass effects
Farhat et al. [57]	Loosely coupled (LC) with nonlinear aeroelastic problems	Simple to implement and computationally inexpensive
		Lack of sufficient time-accuracy and numerical stability
Campbell and Paterson [58]	Tightly coupled (TC) using a fixed-point iteration	Simulated time-dependent pump performance for expandable turbomachinery and demonstrated the need for several sub-iterations
Michler et al. [59]	Monolithic and partitioned method with one-dimensional model of a piston interacting with a fluid	Monolithic scheme is unconditionally stable but computationally expensive
		Computation cost of the partitioned scheme is lower but the interface condition cannot be satisfied exactly
Causin et al. [60]	LC and TC with an incompressible fluid interacting with a thin elastic structure	Simulated the blood flow in large human arteries and reproduced propagation phenomena, taking into account the added-mass effect
Young et al. [61]	Hybrid coupled (HC) modeling forced pitching response of a hydrofoil in fully-wetted flow	Avoids numerical instability issues related to the artificial added mass effects

complex systems [54,55]. While in the partitioned method, the fluid and structural motions are solved independently, and the computational fluid dynamics (CFD) and computational structure dynamics (CSD) are adopted separately, via loosely coupled or tightly coupled methods [54,57–59,62]. However, as discussed in Refs. [60,63,64], the added mass has a significant effect in the partitioned method. The study by Young et al. [61] developed a new hybrid coupling algorithm and simulated the pitching steel/plastic hydrofoils. They evaluated the capability of different partitioned method and found that the new hybrid coupling algorithm has a better convergence and numerical stability.

1.3 Scopes

Although much attention has been paid to the unsteady cavitating flow structures in recent decades, the complex unsteady cloud cavitating flow induced vibration, and the interplay between cavitation and fluid structure interaction makes the cavitation dynamics and hydroelastic response even more complicated. The objectives of this article are to review the recent experimental tools to obtain comprehensive flow field data, and the computational tools for unsteady cavitating flow and its induced vibrations. The emphasis of the simulation is on the homogeneous multiphase model, turbulence closure, and transport cavitation model, along with the coupled fluid structure interaction model. The present review will:

(1) summarize the progress made in the experimental and numerical modeling and approaches for cavitating flows, and cavitation–structure interaction;
(2) discuss the global multiphase structures for different cavitation regimes, with special emphasis on the unsteady development of cloud cavitation, and corresponding cavitating flow-induced vibrations;
(3) improve the understanding of the hydroelastic response in cavitating flows via combined physical and numerical analysis, with particular emphasis on the interaction between unsteady cavitation development and structural deformations.

2 Recent progress for experimental modeling

2.1 Global multiphase structures and associated cavitating flow-induced vibrations

Significant advances of detailed flow measurements have been made in order to obtain an understanding of cavitating flow mechanism. For the transient cavitating flow structures and flow dynamics, with the advent of high-speed digital cameras, the visual observation remains a powerful tool [20,65,66] for most types of cavitation. With the reducing of cavitation number in a specific flow condition (e.g. the given incidence angle of attack, Reynolds number, gas content of the fluid), the cavitating flow displays several patterns:

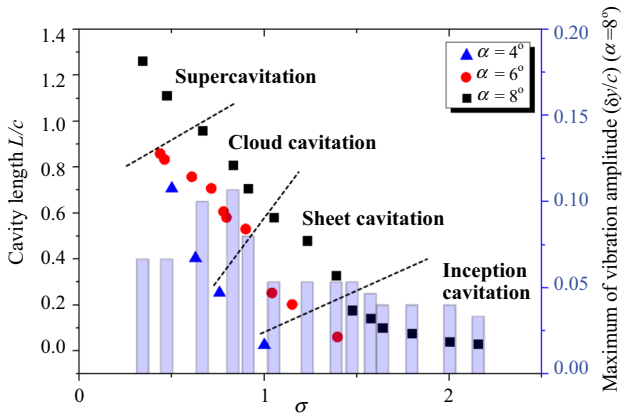

Fig. 1 Normalized cavity length at various angles of attack and cavitation numbers (*the separate points*) and the maximum of the vibration amplitude for different cavitation regimes (*the blue columns*)

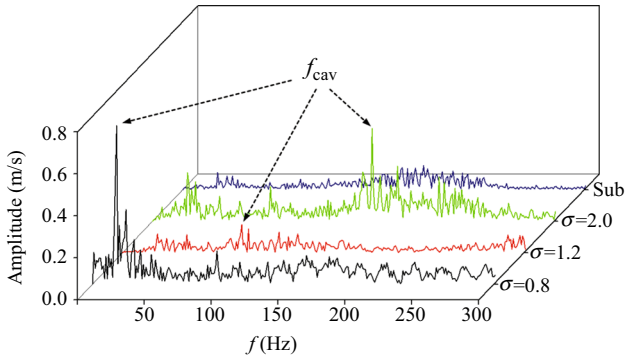

Fig. 2 Effect of cavitation number on the frequency spectrum of vibration velocity

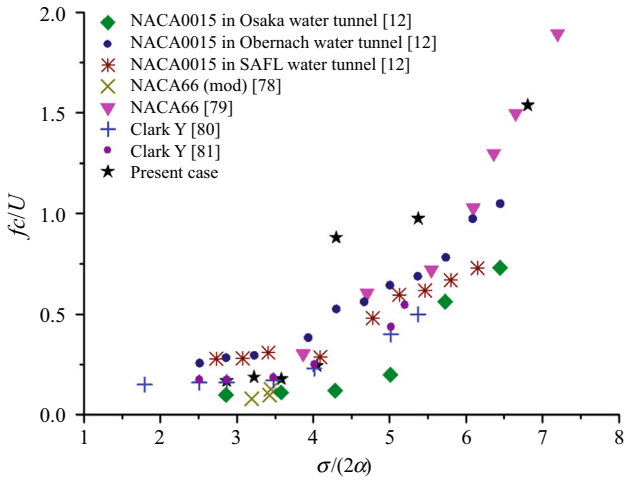

Fig. 3 Main cavity shedding frequencies against $\sigma/(2\alpha)$

incipient cavitation [67,68], sheet cavitation [69,70], cloud cavitation [38,71,72], and supercavitation [73,74].

The appearance of various cavity shapes in different cavitation regimes affects the hydrodynamic performance and is responsible for the generation of structural vibrations. Many experimental studies of vibration measurement can be found in open literature. In Ref. [75], vibration acceleration sensor is used on the centrifugal pump to measure the vibration acceleration at several locations on a casing, suction and discharge pipes. LDV is used to measure the structural vibration velocity according to the heterodyne interferometer principle and has been applied in a wide range of fields [49,76,77]. Figure 1 shows the normalized cavity length at various cavitation numbers and angles of attack (the separate points) and the maximum of the vibration amplitude for different cavitation regimes. Combining the evolution of the cavity length and vibration amplitude evolution for the different cavitation regimes, it is shown that the maximum vibration amplitude stays relatively small for the inception cavitation and sheet cavitation, where the rear region of the sheet cavity is unsteady and rolls up into a series of bubble eddies that shed intermittently. The vibration amplitude increases dramatically for the cloud cavitation, mainly because of the increasing unsteadiness of cavity structures around the hydrofoil. After that, when cloud cavitation transits to supercavitation, the cavitating area covers the entire hydrofoil, extending to the downstream region, and a sharp decline of the vibration amplitude can be observed.

To investigate cavity-induced vibration of hydrofoils for various cavitation regimes, Fig. 2 shows the spectral characteristics of the measured vibration velocity under different cavitation regimes. The main flow-induced frequencies are accordance with the cavity shedding frequency, and such components are not visible in the spectra of fully turbulent flow cases. The main frequency reduces with the decrease of cavitation number because the cavity length increases which requires more time to evolve between subsequent cycles.

The reduced cavity shedding frequency fc/U against $\sigma/(2\alpha)$ is plotted in Fig. 3, including the present results and previous experimental measurements for different hydrofoils [12,77,79–81]. Overall, similar trends can be observed for all cases, with the reduced cavity shedding frequencies keeping constant when $\sigma/(2\alpha) < 4$ and increasing with $\sigma/(2\alpha)$ when larger $\sigma/(2\alpha) > 4$. In addition, similar trends have also been obtained with a Venturi-type section, with scale effects on the periodic cloud shedding considered [70,82].

2.2 Cloud shedding process and associated cavitating flow-induced vibration

Among the different cavitation stages, cloud cavitation often occurs violently and causes more vibration and strong dynamic instabilities [83–85]. The studies by Kubota et al. [10], Kawanami et al. [7], Ji et al. [86], Huang and Wang [87], and Peng et al. [88] paid special attention to the unsteady characteristics of cloud cavitation.

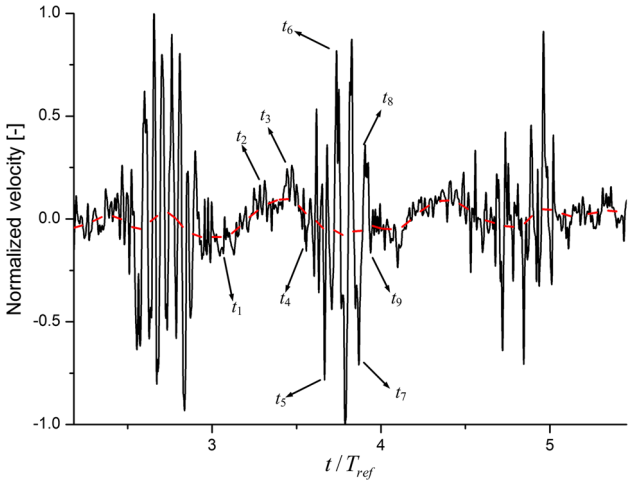

Fig. 4 Evolution of the normalized vibration velocity for the cloud cavitating flow (stainless steel hydrofoil, $\sigma = 0.8$) [89]

To investigate the correlation between the unsteady cavitation behaviors and the flow-induced vibration better, a simultaneous sampling system, which combines the high-speed visualization system and the vibration measurement system with a controller, has been applied in the experiments [89]. Figure 4 shows the time evolution of the vibration velocity of an NACA66 hydrofoil, followed by the evolution of cavity shapes, as shown in Fig. 5. The vibration velocity increases with the growth of the attached cavity. At moment (t_5), the cloud cavity breaks from the attached cavity, the vibration velocity hits the trough. After that, the trend of the vibration velocity almost remains steady while several large amplitude fluctuations of the vibration velocity are observed, which is due to the collapse of the large-scale cloud cavity. According to Huang et al. [90], as shown in Fig. 6, the cloud cavity split at the head of the U-shape and the individual vapor structure collapses toward the foil surface. As the cloud cavity collapses, the propagated pressure pulse released by the cavity collapse aggravates the vibration, corresponding to the peaks and troughs of the vibration velocity. This is also confirmed by Knapp et al. [2], Kato et al. [91], and Chen et al. [51]. Finally, from t_7 to t_9, the cavity sheds downstream with the flow, with the fluctuation amplitude of the vibration velocity decreasing.

3 Recent progress for numerical modeling and approaches

Various issues related to unsteady cavitation should be addressed via combined experimental approaches and computational modeling. The early studies of computational modeling mainly use the potential flow theory, which is still widely applied in many engineering problems [92,93]. Research dealing with cavitation modeling by solving the N–S equations has emerged in the last decade. Different turbulence and cavitation models are listed in this section, for their merits and weaknesses together with detailed effect of unsteady cavitation dynamics.

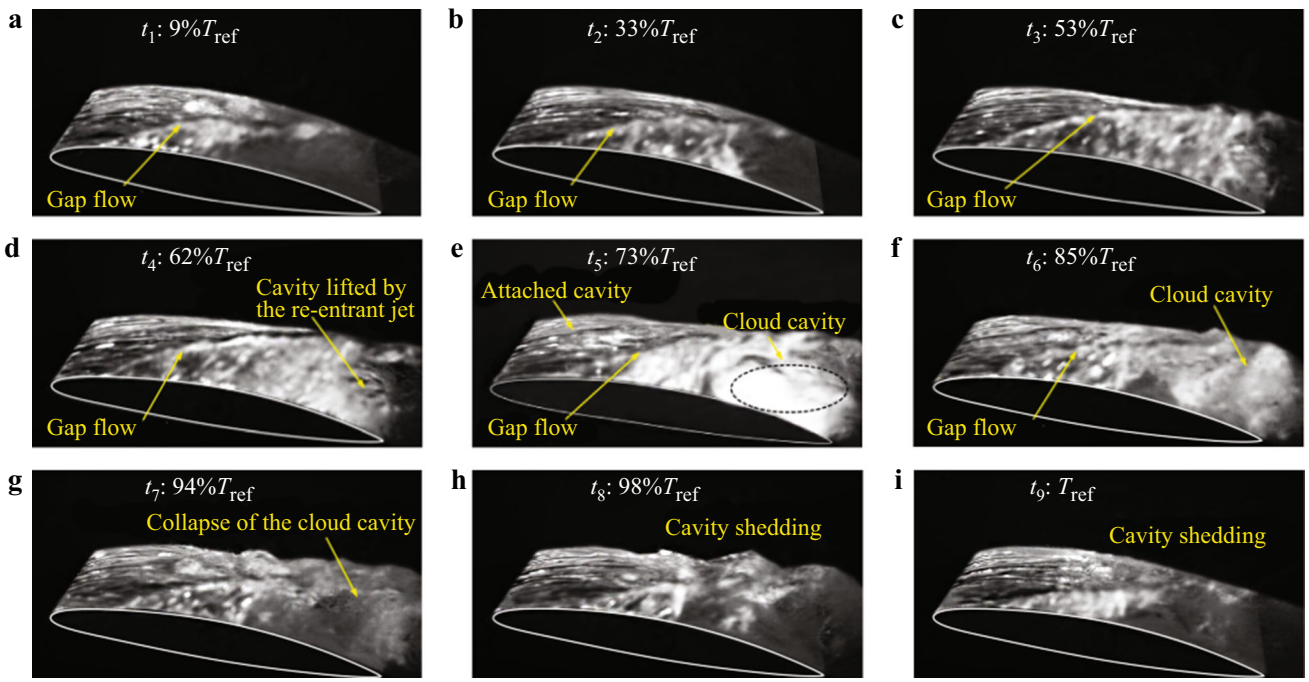

Fig. 5 Time evolution of the cloud cavitation patterns

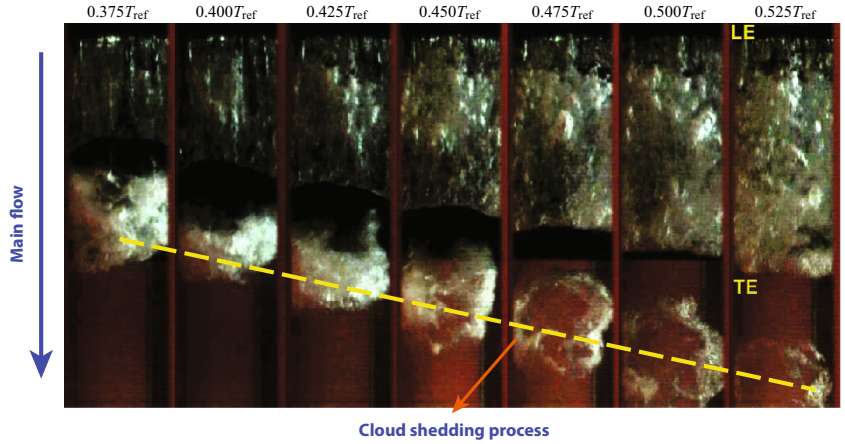

Fig. 6 Observation of the time sequence of photographs of a cloud cavity ($\sigma = 0.8,\ Re = 7 \times 10^5, \alpha = 8°$)

3.1 Cavitation models

Recent cavitation models are categorized as (1) interface tracking method, (2) barotropic cavitation models, (3) transport cavitation models. In the first category, the pressure in the cavity region is assumed to be constant, which is physically sensible and has been verified experimentally [72,94]. Computationally, the interface between the liquid and vapor can be tracked based on this assumption, along with a wake model to handle the cavity shapes. Although the distinct interface can be acquired, the performance of this model is limited seriously if detached cavity exists and also limited to the 3D interfaces [30,95].

In addition to the interface tracking method, the other two methodologies use homogeneous equilibrium flow models for both liquid and vapor phases. In the second category, the local mixture density (ρ_m) is assumed to depend only on the local pressure: $\rho_\mathrm{m} = f(p)$. Reference [17] shows that vorticity production is an important aspect of cavitating flows and is a consequence of the baroclinic torque $\nabla(1/\rho_\mathrm{m}) \times \nabla p$, but the barotropic state equation leads to zero baroclinic torque, so that it cannot properly predict the dynamics of cavitating flows [25].

For these methods above, they did not consider the convection and transport phenomenon of the cavitation due to the lack of cavitation transport equation. In the present article, we mainly refer to the transport-based cavitation models, in which the mass transfer rate can be expressed as

$$\frac{\partial \rho_\mathrm{l}\alpha_\mathrm{l}}{\partial t} + \frac{\partial(\rho_\mathrm{l}\alpha_\mathrm{l}u_j)}{\partial x_j} = \dot{m}^+ + \dot{m}^-. \tag{1}$$

The source ($\dot{m}^+$) term and sink ($\dot{m}^-$) term represent the condensation rate and evaporation rate, respectively.

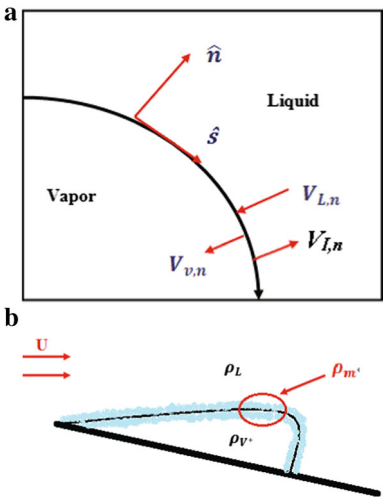

Fig. 7 **a** Schematic of a liquid–vapor interface. **b** Representation of a vaporous cavity in homogeneous flow theory. Model detail can be referred to Ref. [25]

3.1.1 Interfacial dynamic models

Figure 7a shows an interface between the liquid and vapor schematically, and Fig. 7b illustrates a typical liquid-vapor interface based on the homogeneous flow. The work by Senocak and Shyy [25] have neglected the viscous and surface tension forces, the mass and normal momentum conservation conditions reduces to the following forms

$$\rho_\mathrm{l}(V_{\mathrm{L},n} - V_{\mathrm{I},n}) = \rho_\mathrm{v}(V_{\mathrm{v},n} - V_{\mathrm{I},n}) = \rho_\mathrm{m}(V_{\mathrm{m},n} - V_{\mathrm{I},n}), \tag{2}$$

$$P_\mathrm{v} - P_\mathrm{l} = \rho_\mathrm{m}(V^-_{\mathrm{m},n}V_{\mathrm{I},n})^2 - \rho_\mathrm{v}(V^-_{\mathrm{v},n}V_{\mathrm{I},n})^2, \tag{3}$$

where $V_{\mathrm{L},n}$ is the normal velocity of the liquid moving toward the interface, $V_{\mathrm{v},n}$ is the normal velocity of the vapor moving away the interface, $V_{\mathrm{m},n}$ is the normal velocity of the mixture, and $V_{\mathrm{I},n}$ is the normal velocity of the interface.

Based on the continuity and force balance on the interfacial dynamics, the source ($\dot{m}^+$) and sink ($\dot{m}^-$) terms in Eq. (1) can be expressed as the function of the interfacial velocity terms

$$m^+ = \frac{\max(P_\mathrm{l} - P_\mathrm{v}, 0)(1-\alpha_\mathrm{l})}{(V_{\mathrm{v},n}^- V_{\mathrm{I},n})^2(\rho_\mathrm{l} - \rho_\mathrm{v})t_\infty}, \tag{4}$$

$$m^- = \frac{\rho_\mathrm{l}\min(P_\mathrm{l} - P_\mathrm{v}, 0)\alpha_\mathrm{l}}{\rho_\mathrm{v}(V_{\mathrm{v},n}^- V_{\mathrm{I},n})^2(\rho_\mathrm{l} - \rho_\mathrm{v})t_\infty}. \tag{5}$$

The normal component of the vapor velocity $V_{\mathrm{v},n}$ is calculated as

$$V_{\mathrm{v},n} = \boldsymbol{u}\cdot\boldsymbol{n}, \quad \boldsymbol{n} = \frac{\nabla\alpha_\mathrm{l}}{|\nabla\alpha_\mathrm{l}|}. \tag{6}$$

Previous studies expressed $V_{\mathrm{I},n}$ in terms of part of the $V_{\mathrm{v},n}$ [26,27]. Alternate methods of modeling are also discussed by Wu et al. [40], which is based on the evolution of liquid volume fraction.

In spite of the eliminations of empirical constants, this model often predicts a larger cavity size, and the calculation of velocities on the moving interface needs to be improved.

3.1.2 Rayleigh–Plesset bubble dynamic models

The interfacial dynamic cavitation model above come from the dynamics balance in the interface, they still have no connection to the bubble dynamics which dominate the bubble collapse and growth in the cavitation phenomenon. The bubble dynamics can be expressed as simplified form of Rayleigh–Plesset equation, which neglects the acceleration of bubble growth rate, viscous force, and surface tension. It assumes the phase change mainly depends on the pressure difference and the growth of the bubble radius R (seen in Fig. 8) can be given as

$$\frac{\mathrm{d}R}{\mathrm{d}t} = \pm\left(\frac{2}{3}\frac{|P_\mathrm{b} - P|}{\rho_\mathrm{l}}\right)^{0.5}. \tag{7}$$

The Kubota model [97] is a transport-equation based cavitation model assuming a constant nuclei size and nuclei density. The source and sink terms are defined as follows

$$\dot{m}^- = -C_\mathrm{dest}\frac{3\alpha_\mathrm{nuc}(1-\alpha_\mathrm{v})\rho_\mathrm{v}}{R}\left(\frac{2}{3}\frac{p_\mathrm{v} - p}{\rho_\mathrm{l}}\right)^{1/2}, \quad p < p_\mathrm{v}, \tag{8}$$

$$\dot{m}^+ = C_\mathrm{prod}\frac{3\alpha_\mathrm{v}\rho_\mathrm{v}}{R}\left(\frac{2}{3}\frac{p - p_\mathrm{v}}{\rho_\mathrm{l}}\right)^{1/2}, \quad p > p_\mathrm{v}, \tag{9}$$

where α_nuc is the nucleation volume fraction, p is the local fluid pressure, p_v is the saturated vapor pressure, R_B is the bubble diameter. C_dest and C_prod are the constant rate for vaporization and condensation. The model constants can be referred to Ref. [97].

Studies by Singhal et al. [34] and Li et al. [15] used different empirical constants for the phase change rates. The empirical constants of the Singhal model consider the interaction between liquid and vapor phases and the mass transfer rate is assumed to be related to the local turbulence kinetic energy k. Also, Ducoin et al. [98] and Huang et al. [99] evaluated the prediction capability of various popular transport equation-based cavitation models for the simulations of quasi-steady and unsteady cavitating flows around the stationary and pitching NACA66 hydrofoil. Generally speaking, those empirical constants are still limiting the accuracy as a noise loading.

3.2 Turbulence closures

The interplay between cavitation and turbulence is important for the cavitation investigations.

The original $k-\varepsilon$ turbulence model was proposed by Launder and Spalding [100] and has become popular for practical engineering flow calculations. But the original $k-\varepsilon$ model was not intended for highly compressible and multiphase flow. Previous research [38] has shown that the two-equation model always over-predicts the turbulence kinetic energy, and hence turbulent viscosity, causing the

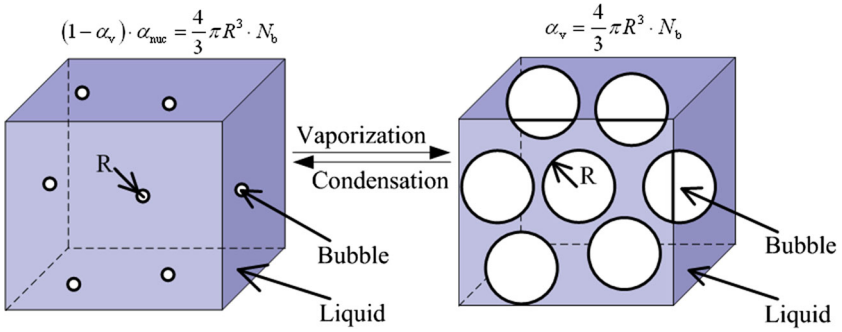

Fig. 8 Schematic diagram of evaporation and condensation [96]

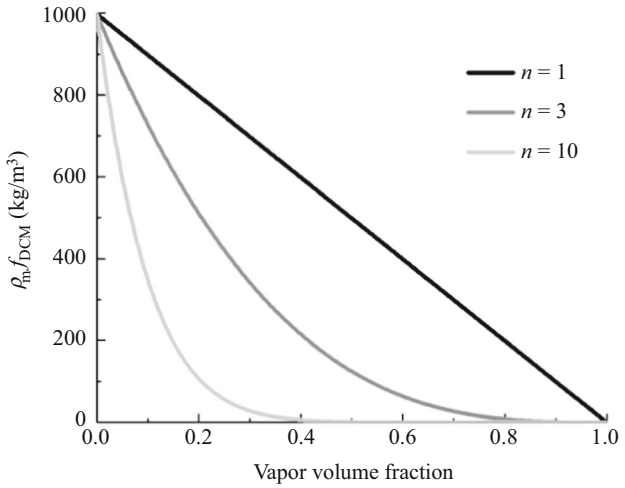

Fig. 9 Local compressibility with different n values

re-entrant jet not to be able to cut across the sheet cavity, which significantly modifies the cavity shedding behavior. Hence, a systematic method to lower the turbulent viscosity in the vapor region is necessary to improve the prediction of the reentrant jet and vapor dynamics in unsteady cavitating flows

To account for the effect of local compressibility effect on the turbulent closure model, the density corrected model (DCM) proposed by Reboud et al. [41] and Coutier-Delgosha et al. [38] is used, seen in Eq. (10):

$$\mu_{T\_DCM} = \frac{C_\mu \rho_m k^2}{\varepsilon} f_{DCM}, \quad C_\mu = 0.09,$$
$$f_{DCM} = \frac{\rho_v + (1-\alpha_v)^n(\rho_l - \rho_v)}{\rho_v + (1-\alpha_v)(\rho_l - \rho_v)}. \tag{10}$$

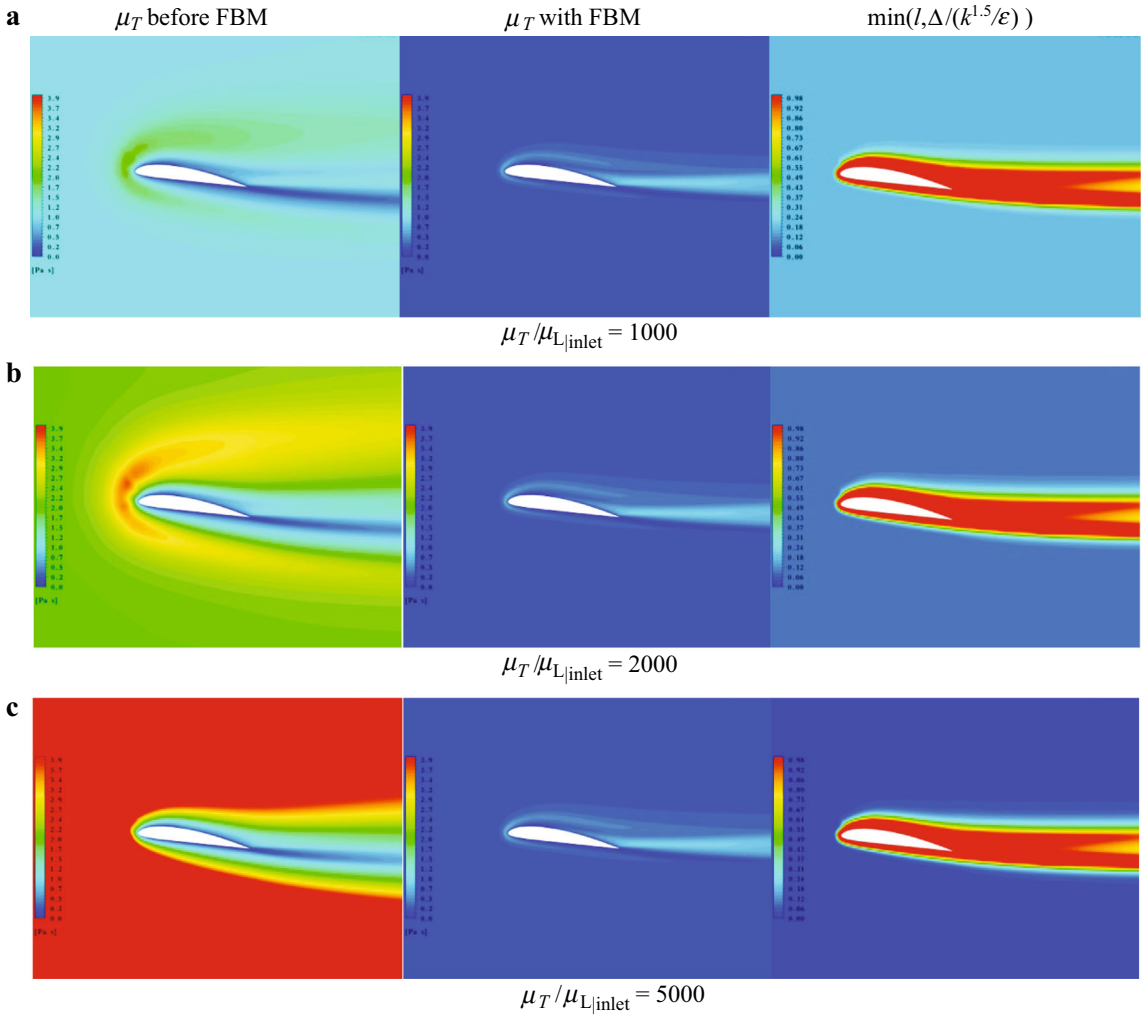

Fig. 10 Comparisons before/after FBM for Clark-Y hydrofoil ($\sigma = 1.40$)

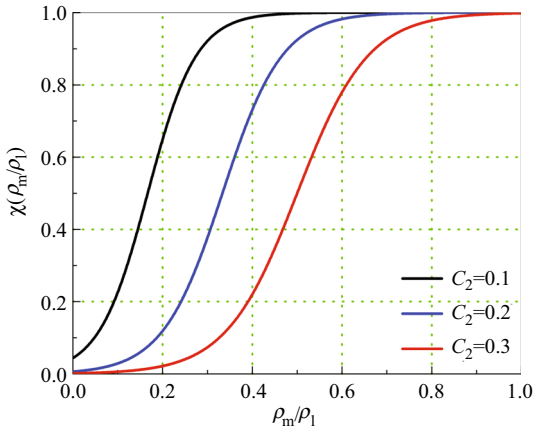

Fig. 11 Distribution of the hybrid function χ for the FBDCM model according to Eq. (13)

The variation of the modified effective density, $\rho_m f_{DCM}$ for different values of n is shown in Fig. 9. The studies by Coutier-Delgosha et al. [38] and Ducoin et al. [98] recommended values of n with a focus on the specific part of the cavitation developing process.

Furthermore, Johansen et al. [43] proposed an FBM, with the turbulent eddy viscosity modified by a filter function:

$$\mu_{T\_FBM} = \frac{C_\mu \rho_m k^2}{\varepsilon} f_{FBM}, \quad C_\mu = 0.09,$$
$$f_{FBM} = \min\left(1, \frac{\lambda \cdot \varepsilon}{k^{3/2}}\right). \tag{11}$$

The FBM model helps to limit the turbulent eddy viscosity in the cavitating wake region, where many other turbulence models are not effective because of the low vapor fraction in the shed cloud cavity. Hence, it can better predict the cavitating wake dynamics.

The work by Tseng and Shyy [22] presented isothermal water cavitation and displayed the interaction between turbulence and cavitation models. They pointed out that the numerical results depend on the inlet turbulent quantities at inlet, which affects the pressure distribution and also cavitation development. Figure 10 explains how the filter in FBM model helps to weaken the result sensitivity with respect to the inlet conditions. For the RANS model, the eddy viscosity contours change noticeably with the increase of eddy-to-laminar viscosity ratio at the inlet. While for FBM model, the higher the inlet eddy-to-laminar viscosity ratio, the lower the filter function in FBM, and the numerical results showed less dependence on the eddy viscosity.

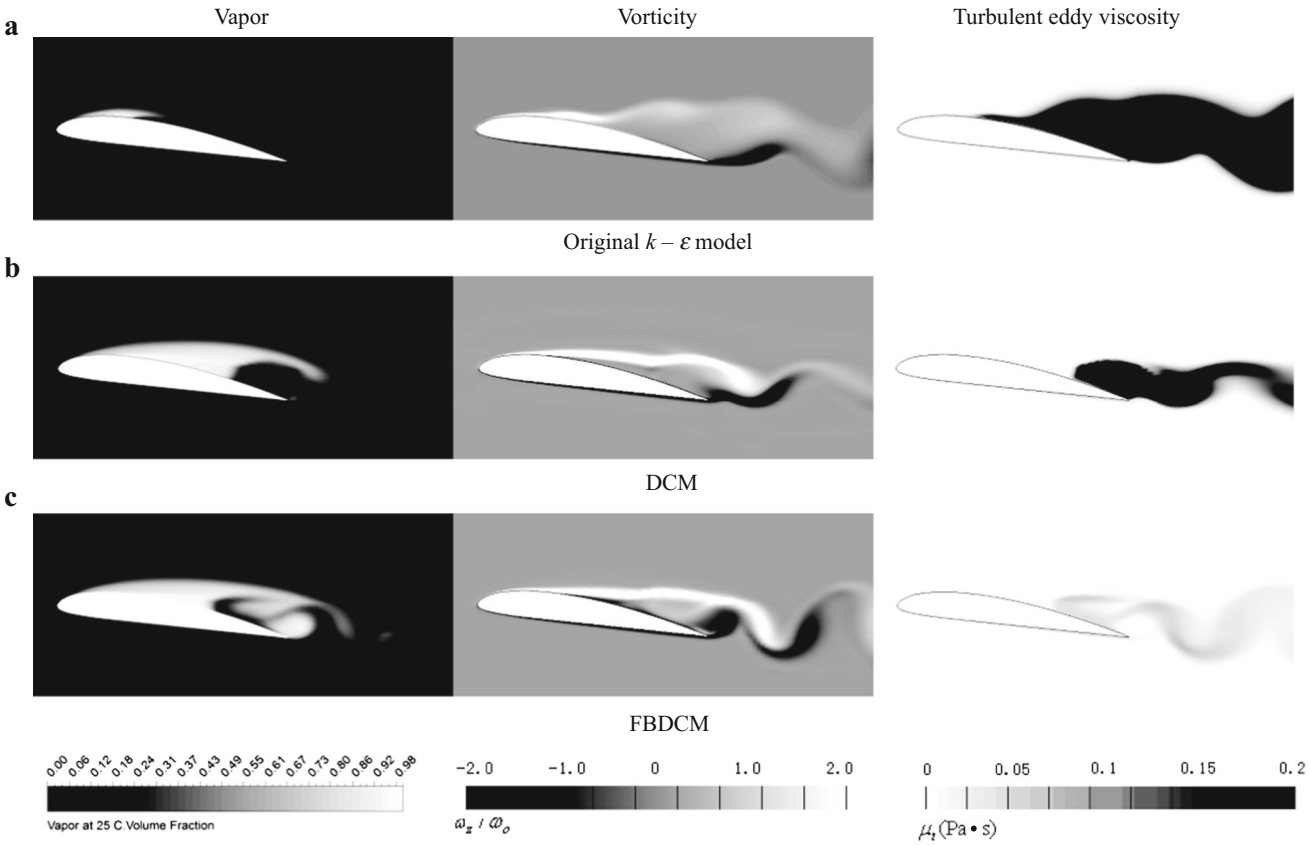

Fig. 12 Comparison of the predicted vapor volume fraction, vorticity, and turbulent eddy viscosity contours obtained via the original $k-\varepsilon$ model, DCM and FBDCM approaches at $0.625T_{ref}$ for $\sigma = 0.8$, $Re = 7 \times 10^5$, and $\alpha = 8°$ [90]

Table 4 Comparison of the vortex shedding frequencies predicted by different turbulence models

	Experiment	$k-\varepsilon$ model	DCM	FBDCM
Mean value f (Hz)	69.2	25.5	46.5	72.0

As the FBM and DCM approaches are designed to decrease the turbulent eddy viscosity in different regions, a filter-based density corrected model (FBDCM) that combines the strengths of both models is proposed to limit the turbulent eddy viscosity in the cavitating wake region and the cavitation region near the foil surface, which replaces μ_T with μ_{T_hybrid}:

$$\begin{aligned}\mu_{T\_\text{hybrid}} &= \frac{C_\mu \rho_\text{m} k^2}{\varepsilon} f_\text{hybrid}, \quad C_\mu = 0.09,\\ f_\text{hybrid} &= \chi(\rho_\text{m}/\rho_\text{l}) f_\text{FBM} + [1-\chi(\rho_\text{m}/\rho_\text{l})] f_\text{DCM}, \qquad (12)\\ \chi(\rho_\text{m}/\rho_\text{l}) &= 0.5 \\ &\quad + \tanh\left[\frac{C_1(0.6\rho_\text{m}/\rho_\text{l} - C_2)}{0.2(1-2C_2)+C_2}\right] \Big/ [2\tanh(C_1)], \qquad (13)\end{aligned}$$

where the constant value of C_1 and C_2 are optimized with surrogate model [101–103]. It is revealed that the performance of the filter-based density correction model is affected more by model parameter C_2, which is used to regulating the proportion of FBM and DCM based on local mixture density (seen in Fig. 11), so that it will help to limit the over-prediction of the turbulent eddy viscosity in the cavitating regions on the foil wall and in the wake. With the recommended model parameter values, $C_1 = 4$ and $C_2 = 0.2$, better prediction of the cavitating flows can be attained [104].

Figure 12 compares the effectiveness of the different turbulence models for unsteady sheet/cloud cavitating flows at $t = 0.625T_\text{cycle}$. The original $k-\varepsilon$ model over-predicted the turbulent eddy viscosity in the cavitating region and the wake region, which affects the prediction of the cavity shedding process and vortex structure interactions in the wake. The DCM model reduced the turbulent eddy viscosity in the cavity region near the wall, and the FBDCM model reduced the turbulent eddy viscosity in both the cavity and the wake region, which allowed the cavity to shed and the trailing edge vortex to be fully developed and interacted with the shedding cloud cavities, which is critical to the prediction capability. Comparisons of the measured and predicted vortex shedding frequencies obtained using the three different turbulence models are listed in Table 4. The value predicted by the original $k-\varepsilon$ model had the largest discrepancy with

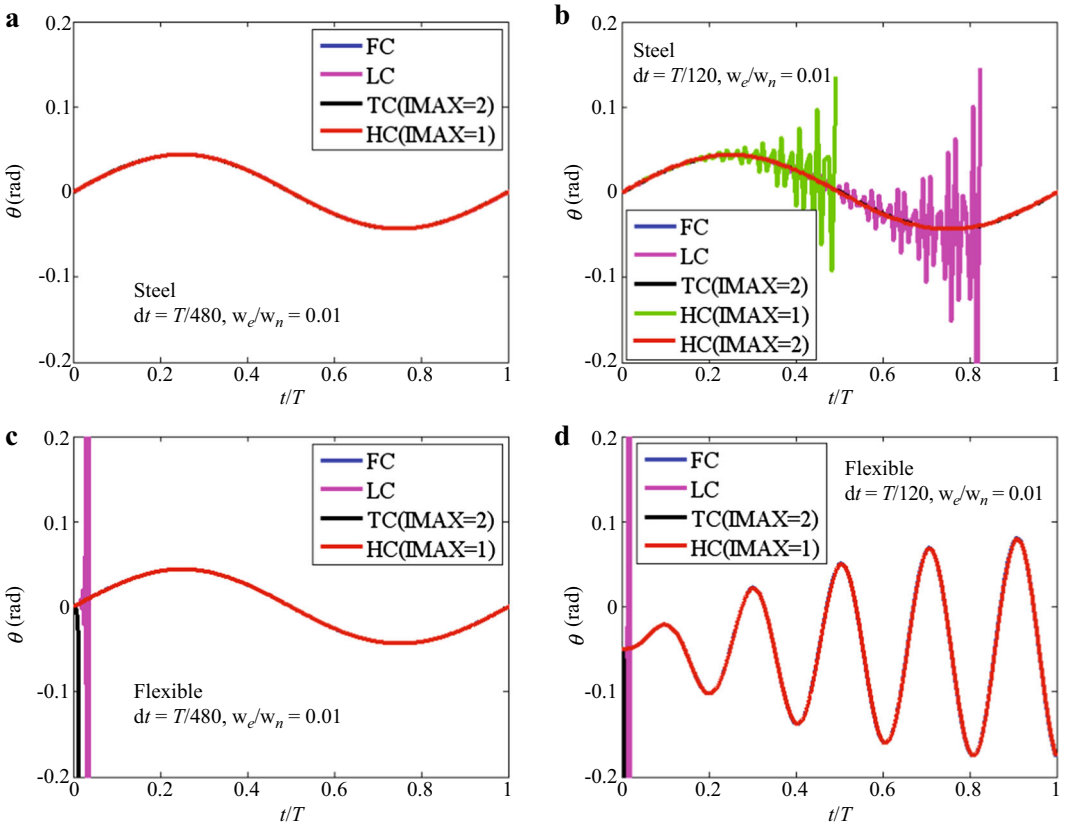

Fig. 13 Different coupled algorithms for modeling 1D fluid structure interaction

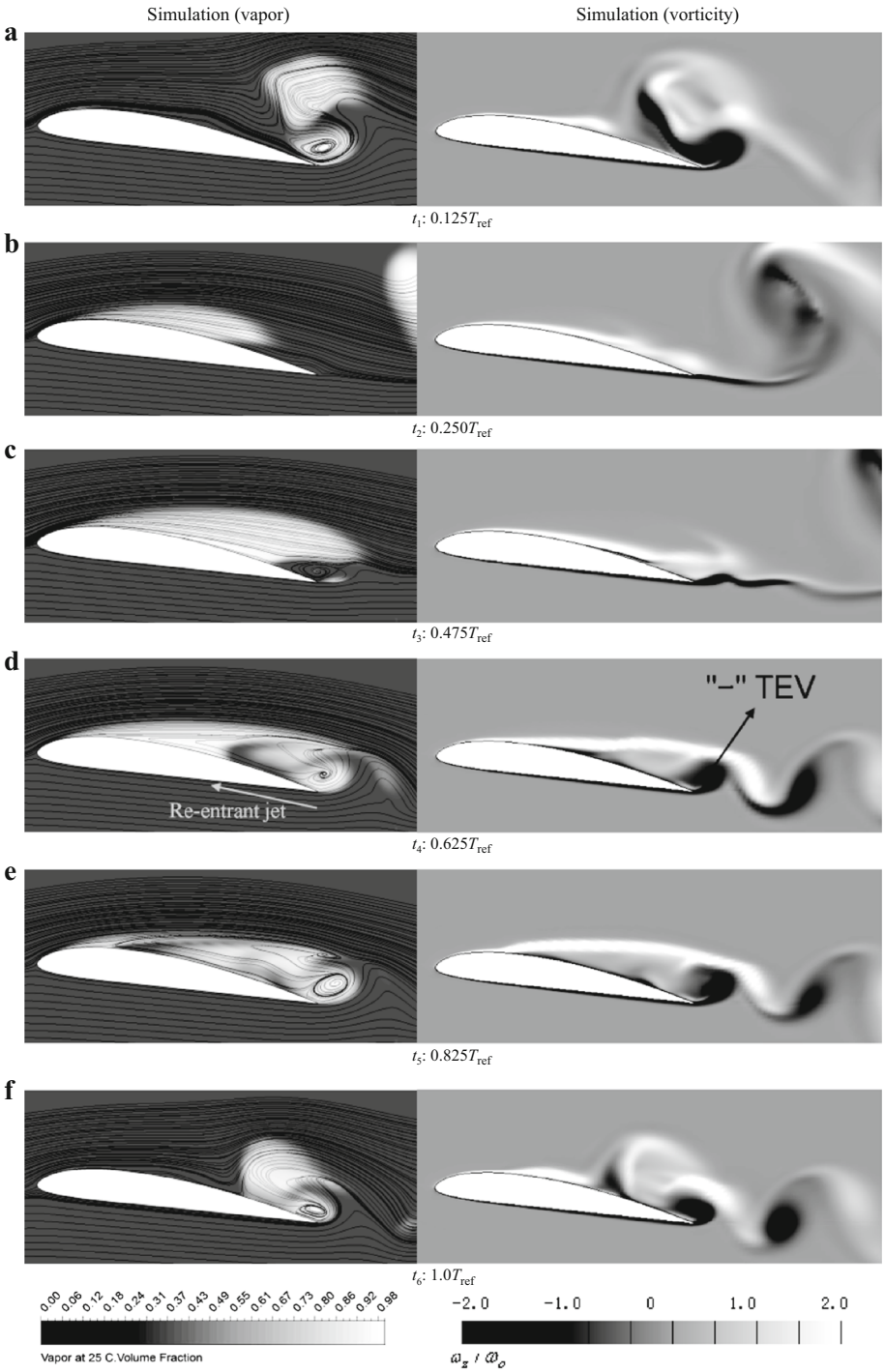

Fig. 14 Predicted vapor fraction contours and vorticity contours ($\sigma = 0.8$, $Re = 7 \times 10^5$, $\alpha = 8°$) [90]

the measured frequency, and the new FBDCM model showed the best agreement with the measured frequency.

3.3 Coupled fluid–structure interaction modeling

Different coupled algorithms for modeling the 1D fluid–structure interaction in viscous flow are compared, as shown in Fig. 13. The fully coupled algorithm is unconditionally stable and considered as a reference results. With small time-step and trivial structure deformation, the results obtained via the loosely coupled algorithm, the tightly algorithm and the hybrid algorithm agree well with the result by fully coupled algorithm. While, by increasing the time-step, or more significantly, structure deformation, as well as the fluid–structure

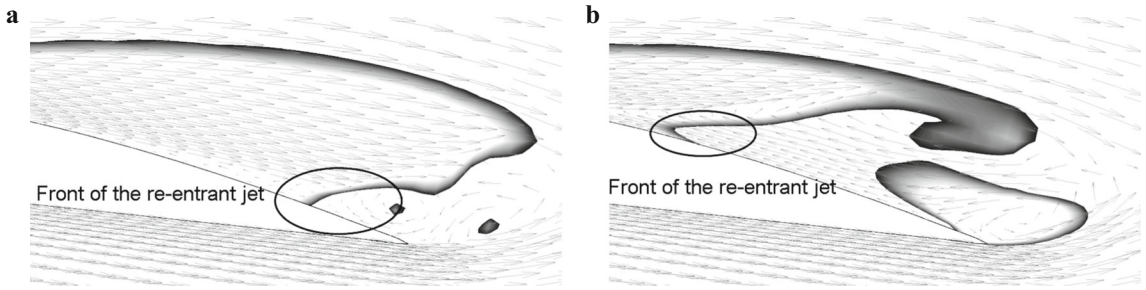

Fig. 15 Formation and development of the re-entrant jet at typical time ($\sigma = 0.8$, $Re = 7 \times 10^5$, $\alpha = 8°$)

interaction, the hybrid-coupled algorithm accounts for the effects of fluid inertial, damping, and restoring forces in each time step so that it is able to improve the numerical stability associated with artificial added mass effects, which are not well considered in loosely/tightly coupled algorithm.

Based on a chord-wise rigid, two-degrees-of-freedom hydrofoil, considering the bending and twisting deformation of the tip section of the hydrofoil, the governing equation without external excitation forces can be expressed as

$$\begin{bmatrix} m & S_\theta \\ S_\theta & I_\theta \end{bmatrix} \begin{Bmatrix} \ddot{h} \\ \ddot{\theta} \end{Bmatrix} + \begin{bmatrix} C_h & 0 \\ 0 & C_\theta \end{bmatrix} \begin{Bmatrix} \dot{h} \\ \dot{\theta} \end{Bmatrix} + \begin{bmatrix} K_h & 0 \\ 0 & K_\theta \end{bmatrix} \begin{Bmatrix} h \\ \theta \end{Bmatrix} = \begin{Bmatrix} L \\ M \end{Bmatrix}, \tag{14}$$

where m is the mass of structure, I_θ, and S_θ are the moment of inertia and the static imbalance, respectively, C_h and C_θ are the structural bending and torsional damping coefficients, K_h and K_θ are the structural stiffness values for bending and twisting motions. h, $\dot{h}$, and $\ddot{h}$ are the bending displacement, velocity, and acceleration, while θ, $\dot{\theta}$, $\ddot{\theta}$ are the twisting displacement, velocity, and acceleration. L_f and M are the lift and moment acted by the flow, which are predicted by the fluid solver, combined with the cavitation models and turbulence closures discussed in Sects. 3.1 and 3.2. In addition, Eq. (14) is solved with Crank–Nicholson method, which is presented and validated in the previous work [105,106].

The equation of motion is discretized as

$$\begin{bmatrix} m & S_\theta \\ S_\theta & I_\theta \end{bmatrix} \begin{Bmatrix} \ddot{h} \\ \ddot{\theta} \end{Bmatrix}_{n+1}^{i+1} + \begin{bmatrix} C_h & 0 \\ 0 & C_\theta \end{bmatrix} \begin{Bmatrix} \dot{h} \\ \dot{\theta} \end{Bmatrix}_{n+1}^{i+1} + \begin{bmatrix} K_h & 0 \\ 0 & K_\theta \end{bmatrix} \begin{Bmatrix} h \\ \theta \end{Bmatrix}_{n+1}^{i+1} - \begin{Bmatrix} L_{\text{fluid}}^T \\ M_{\text{fluid}}^T \end{Bmatrix}_{n+1}^{i+1} = \begin{Bmatrix} L_f \\ M \end{Bmatrix}_{n+1}^{i} - \begin{Bmatrix} L_{\text{fluid}}^T \\ M_{\text{fluid}}^T \end{Bmatrix}_{n+1}^{i}, \tag{15}$$

where L_{fluid}^T and M_{fluid}^T are the hydroelastic force and momentum proposed by Theodorsen [107] and developed by Ducoin et al. [76,108], Young et al. [61], and Wu et al. [77].

4 Unsteady cavitating flow structures

The dynamics of unsteady, turbulent, multiphase cavitating flow is important for understanding the cavitating flow mechanism. Combined physical and numerical analysis has been applied to enhance the understanding of the structures of unsteady sheet/cloud cavitation [109].

As shown in Fig. 14, the numerical results show detailed evolution of the cavity, including the formation, growth, and subsequent shedding, which are in a good agreement with the qualitative features observed in the experiment [87,89]. The effect of the re-entrant flow on the shedding and collapse of large-scale cavitating vortex structure has been mentioned by many researchers [7,12]. Figure 15 highlights the formation and development of the re-entrant jet by numerical simulations at t_3 and t_4 to show the representative unsteady behaviors. The recirculation zone consists of the re-entrant jet in the lower part and mainstream flow in the upper part. The recirculation zone grows in size, meanwhile the re-entrant jet pushes the attached cavity toward upstream, followed by the detach of the cavity. During the process, there is strong interaction between the cloud cavity and the counter-rotating trailing edge vortexes, which can be referred to Ref. [89].

To investigate further the physical mechanism that governs the unsteady sheet/cloud cavitating flow dynamics and structures, the predicted vapor volume fraction of the cavity at mid-span of the foil, as well as the axial velocity (u) and relative higher pressure ($C_p > 0$), are expressed as functions of space and time, as shown in Fig. 16. The cavity shedding process is periodic, and the development of the re-entrant jet triggers the cavity detachment, and the pressure increases immediately when the attached cavity grows to maximum, as shown in Fig. 16c.

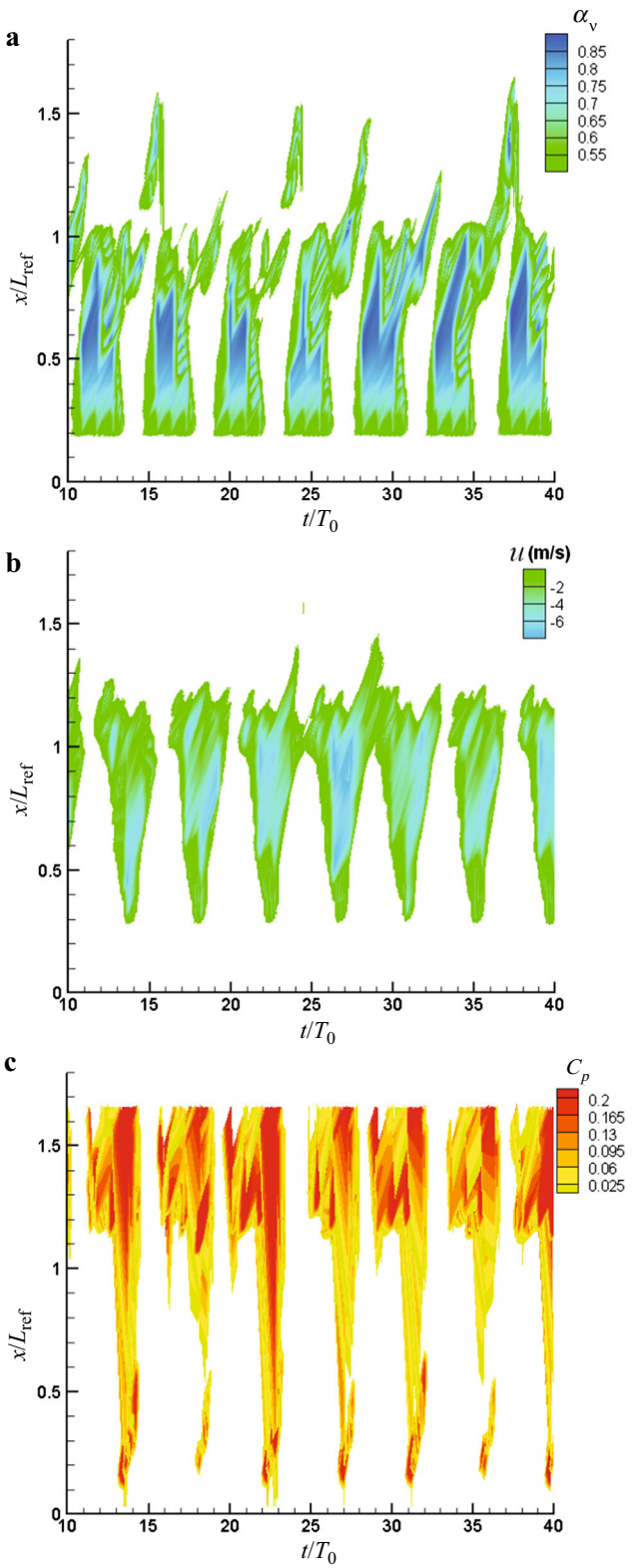

Fig. 16 Numerically predicted time evolution of the **a** water vapor fraction (α_v), **b** reverse u-velocity, and **c** pressure in various sections ($\sigma = 0.8$, $Re = 7 \times 10^5$, $\alpha = 8°$)

5 Influence of hydroelastic response on cavitating flows

With increasing interest in using lighter and more flexible material for many engineering applications, the hydroelastic response has attracted a lot of attention among the turbulent and cavitating flow investigations [110–112]. Compared with the classical aeroelastic problem, the fluid inertia and damping effects cannot be ignored in the hydroelastic response issues, especially when cavitation occurs. Hence, it is of primary importance to study the hydroelastic effect on the cavitation, which is crucial for design and safe operation of the hydraulic machinery and also marine structure systems.

The work by Wu et al. [77] investigated the effect of cavitation on the hydroelastic response. Figure 17 shows the evolution of bending and twisting deformations of a hydrofoil made of polyoxymethylene (POM) in non-cavitating and cavitating flows. Compared with the non-cavitating case shown in Fig. 17a, it is shown that the cavitation enhanced the bending deformation because of the lower pressure in the cavity region on the suction side of the foil, resulting to the larger pressure difference around the hydrofoil.

To investigate further the effect of the hydroelastic response on the unsteady cavitation, including the transient cavitating flow structures and vortex structures, studies for a rigid and a flexible hydrofoil have been conducted.

In the non-cavitating flow, as shown in Fig. 18, the twist deformation causes larger velocity at the leading edge of the hydrofoil, and larger hydrodynamic coefficients [77,78,113]. Further, considering the transition, stall, and static divergence phenomenon occurred in viscous flow, the hydrodynamic and hydroelastic responses of flexible hydrofoils have been compared in Ref. [108].

As for the hydroelastic response in cavitating flow, the structural deformation and dynamics might be strongly coupled with the hydrodynamic cavitation, and also, the collapse of large-scale cloud cavity lead to strong vibration as shown in Sect. 2.2, which makes the cavitation development more complex. As shown in Fig. 19, compared to the periodic development of the hydrodynamic coefficients for the rigid hydrofoil, that for the flexible one are less obviously observed, and fluctuate more significantly.

Based on the dynamic loading evolution, in Ref. [77], flow-induced frequency for flexible hydrofoils is investigated. As shown in Fig. 20, the primary flow-induced frequencies are in agreement with the main cavity shedding frequency, and the secondary flow-induced frequencies are responsible for the vortex shedding frequencies. From the time evolution of the frequency bands shown in Fig. 21, the frequency bands with large amplitude occurred intermittently

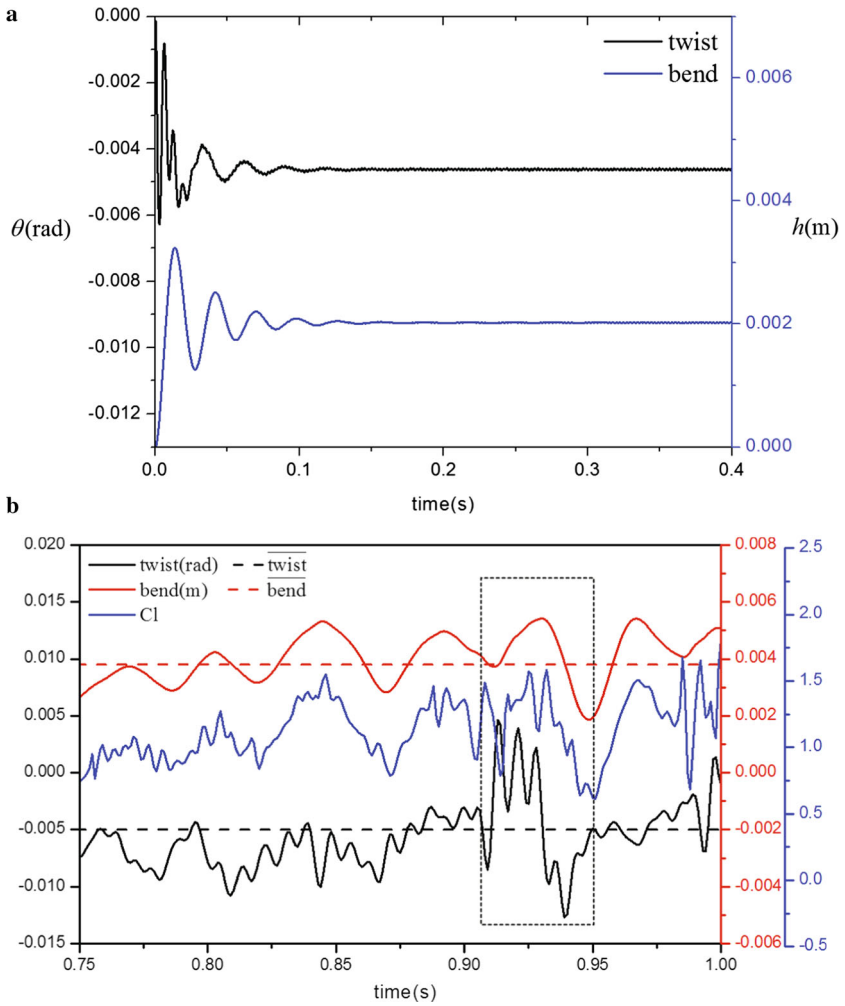

Fig. 17 Comparison of the bending and twisting deformations in **a** non-cavitating flow and **b** cavitating flow [77]

and randomly for the flexible hydrofoil case, which is closely related to the disturbance caused by the structural flutter and deformation, responding to a more complex cavitation pattern discussed as follows.

As for the effect of the hydroelastic response on the detailed cavitation development process and cavitation–vortex interactions, very little work has been accomplished thus far. The work by Wu et al. [77] has divided the process into three stages. During the development of the attached cavity, the pressure center moves toward the leading edge of the flexible foil due to the twist deformation and larger effective angle of attack, as shown in Fig. 22. As shown in Fig. 23, during the vortex structure interaction and cavity shedding stage, Luo et al. [81] presented many detailed results about the re-entrant jet and vortex-cavity interaction, while in Ref. [77], it is found that the hydroelastic response disturbed the unsteady development of cavitation and influenced the leading and trailing edge vortex interactions. When the cloud cavity reaches the trailing edge ($t_6 = t_0 + 40\%T$), the lead-

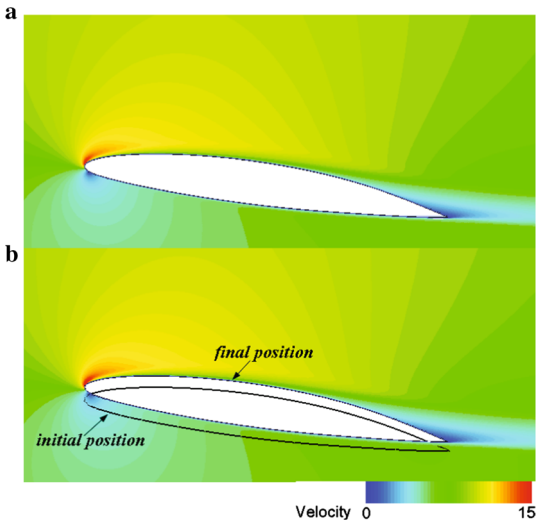

Fig. 18 Velocity contours for rigid/flexible hydrofoil [77]

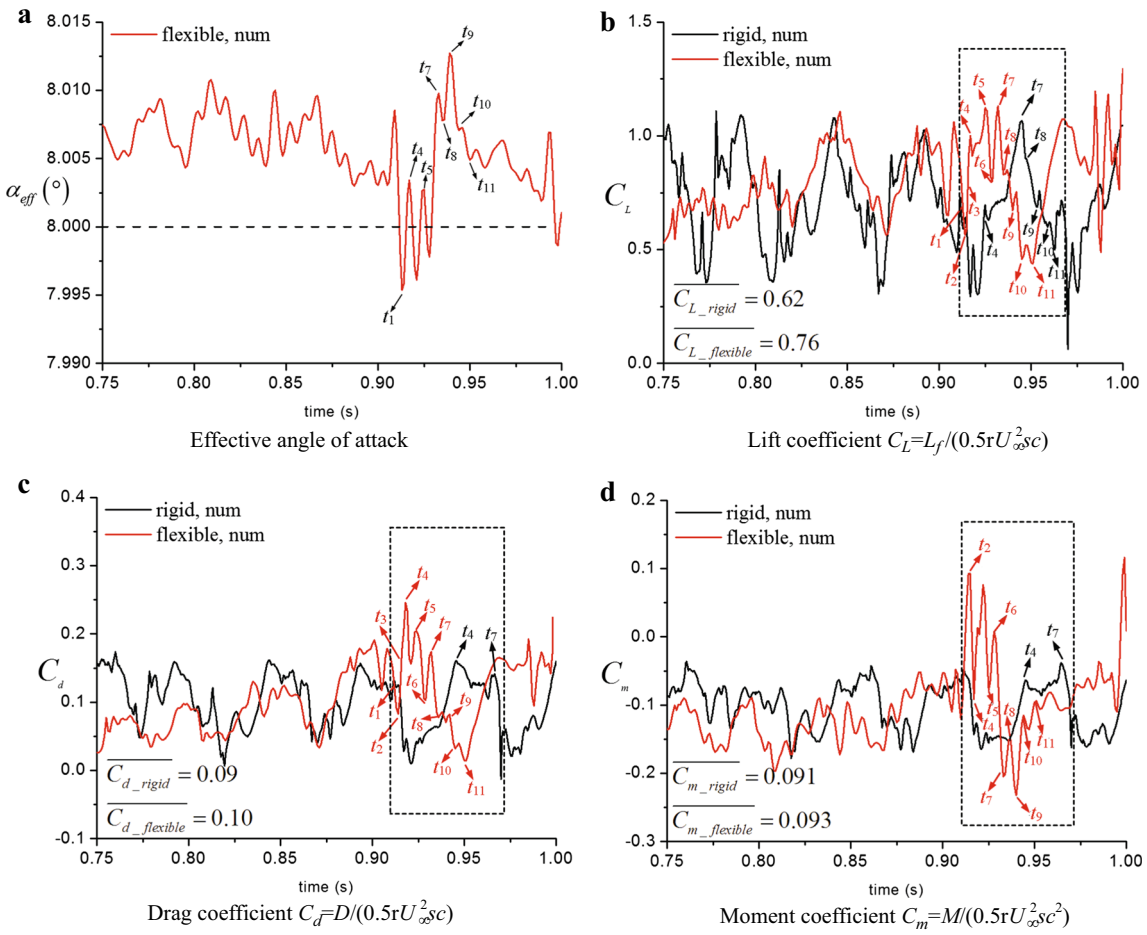

Fig. 19 Evolution of the effective angle of attack for the flexible hydrofoil with time and comparisons of the predicted hydrodynamic load coefficients for the rigid and flexible hydrofoils [77]

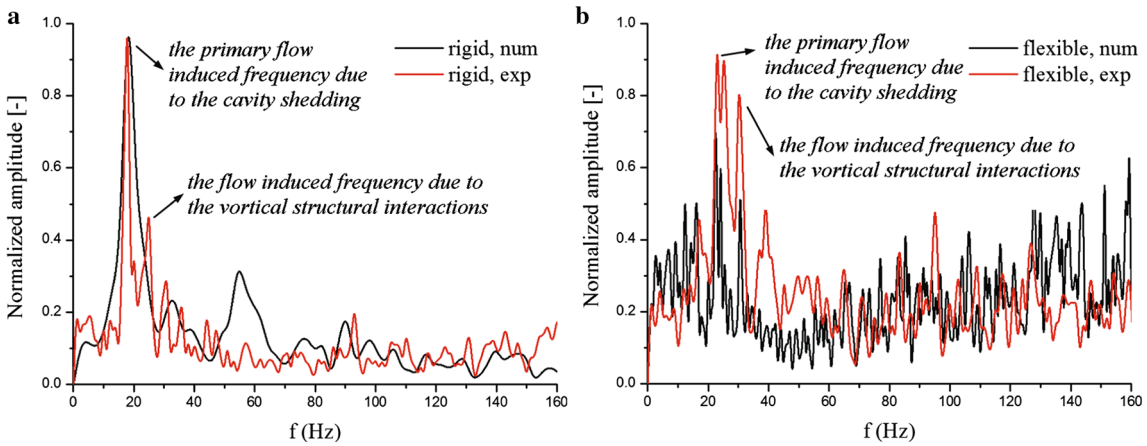

Fig. 20 Spectral characteristics of the vibration acceleration (exp) and the lift coefficient (num) for the rigid and the flexible hydrofoils [77]

ing and trailing edges of the vortex interact with each other, resulting in the shedding of the cavitating vortex structures and interacting with the downstream counter-clockwise vortex again. During the final stage, the primary and residual cavities shed downstream, followed by the formation of the partial sheet cavity for the next period. On one hand, the larger effective angle of attack is caused by the twist deformation, so that the cavity inception of the next period of the flexible hydrofoil is advanced with a higher cavity shedding frequency. On the other hand, instead of shedding as a whole

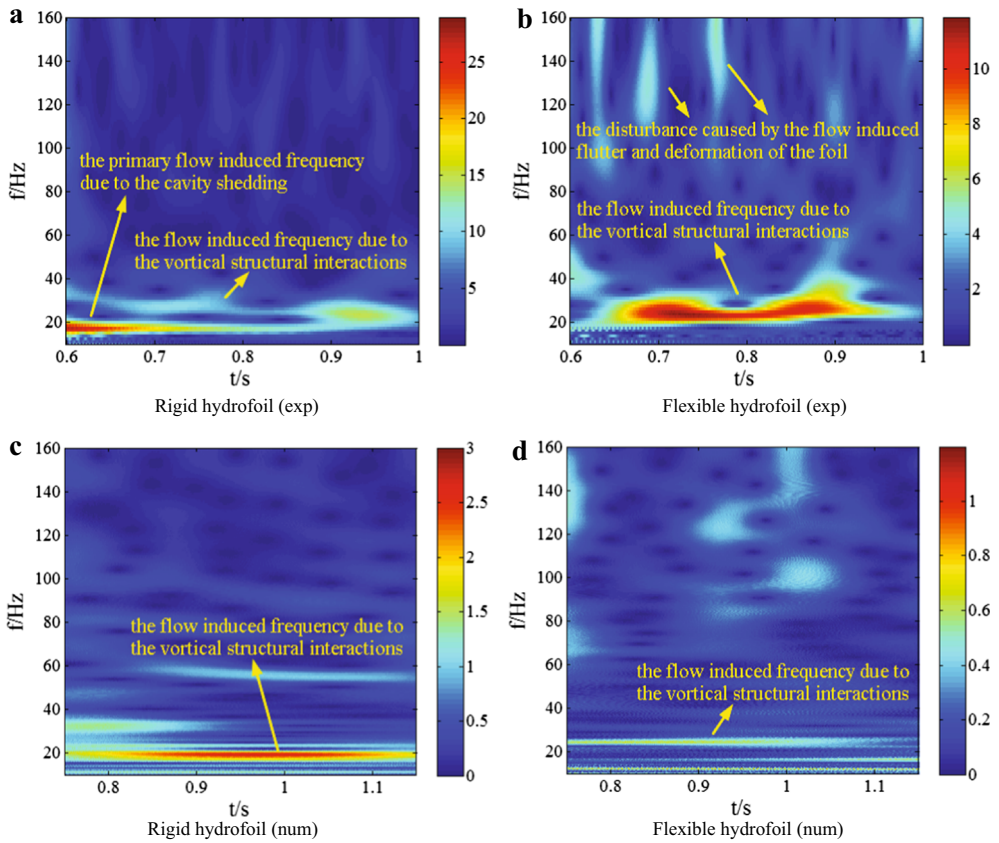

Fig. 21 Spectrograms of the lift coefficient (num) and the vibration acceleration (exp) as a function of time for the rigid and the flexible hydrofoils [77]

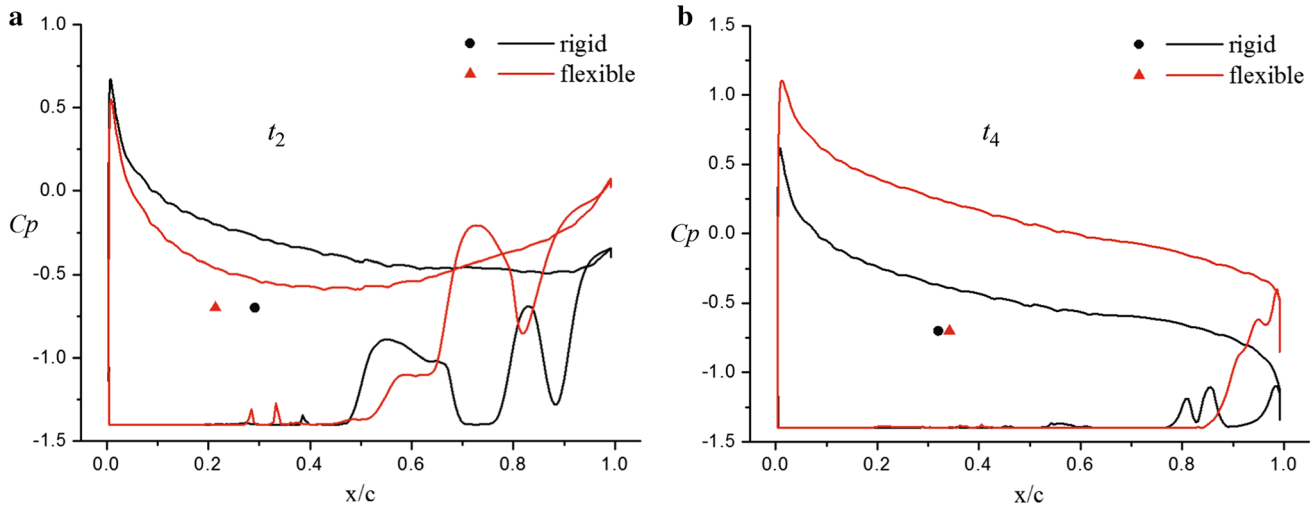

Fig. 22 The pressure distributions and pressure center locations during the development of the attached cavity [77]

cloud cavity for stainless steel hydrofoil, when the cloud cavity reaches to the trailing edge of the flexible hydrofoil, the cavity partially collapses with the vibration and breaks into several medium-scale cloud cavities, which are transported with the flow, as shown in Fig. 24.

6 Future works

Although much progress has been made on experimental and numerical modeling of cavitation and cavitating flow-induced vibrations, further improvement is still necessary.

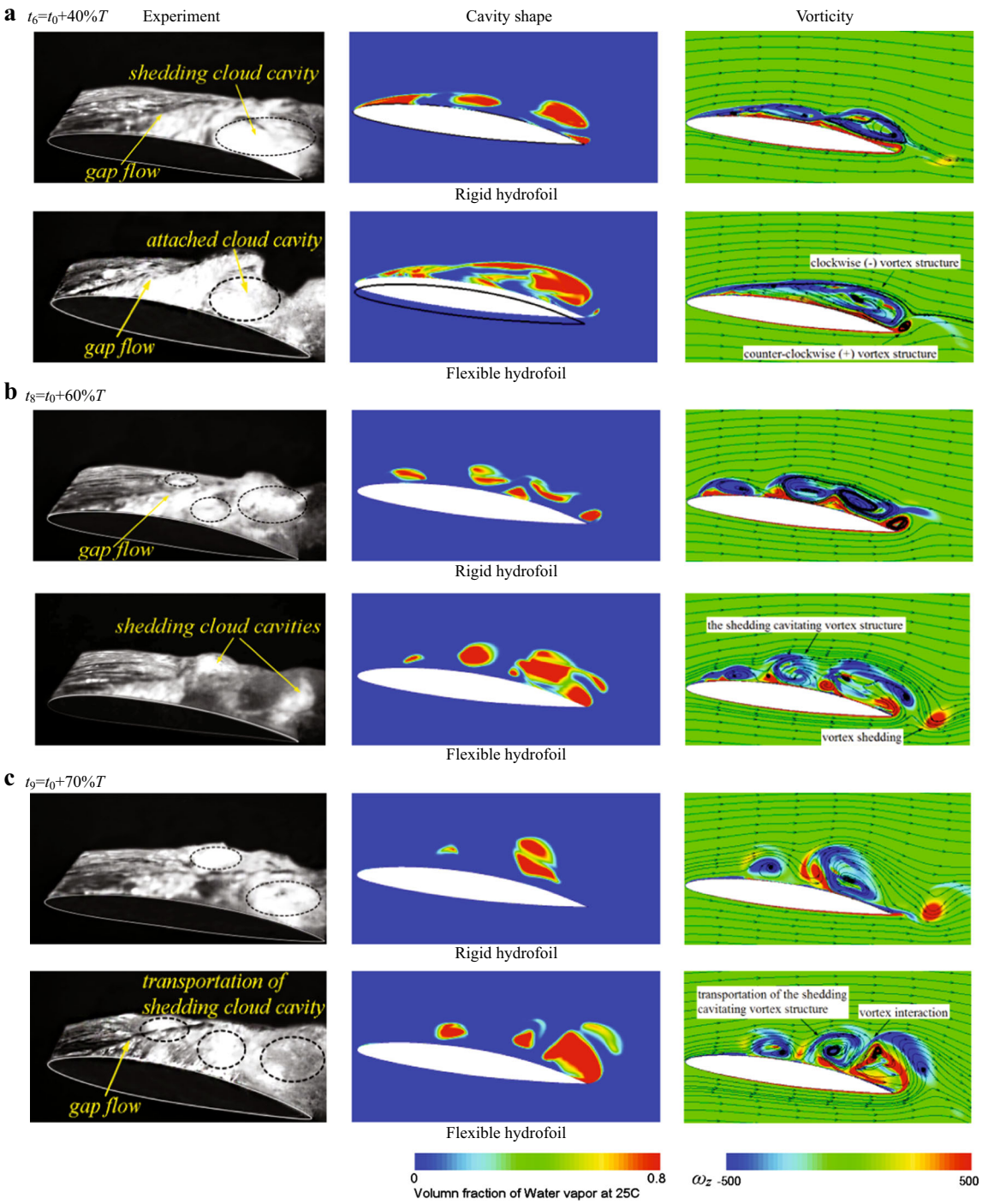

Fig. 23 Evolution of cavitation patterns for the flexible and rigid hydrofoils [77]

Much effort has been made to explain the physics of cavitation in connection with various phenomena such as turbulence, multiphase flow, viscosity and boundary layer, compressibility, and so on. Particularly, the liquid compressibility has great effect on the final stage of bubble collapse, which causes the emission of shock waves and acoustic waves. While one of the main difficulties occurring in the numerical simulation is related to the compressibility of the multiphase flow in the quasi-incompressible flow behavior. It is of significant importance to consider the compressibility of the vapor and liquid-vapor mixture in the numerical model.

Experimental technique is of primary importance not only for the unsteady cavitating flow patterns and dynamics, but also for the cavitating flow-induced vibrations. Though

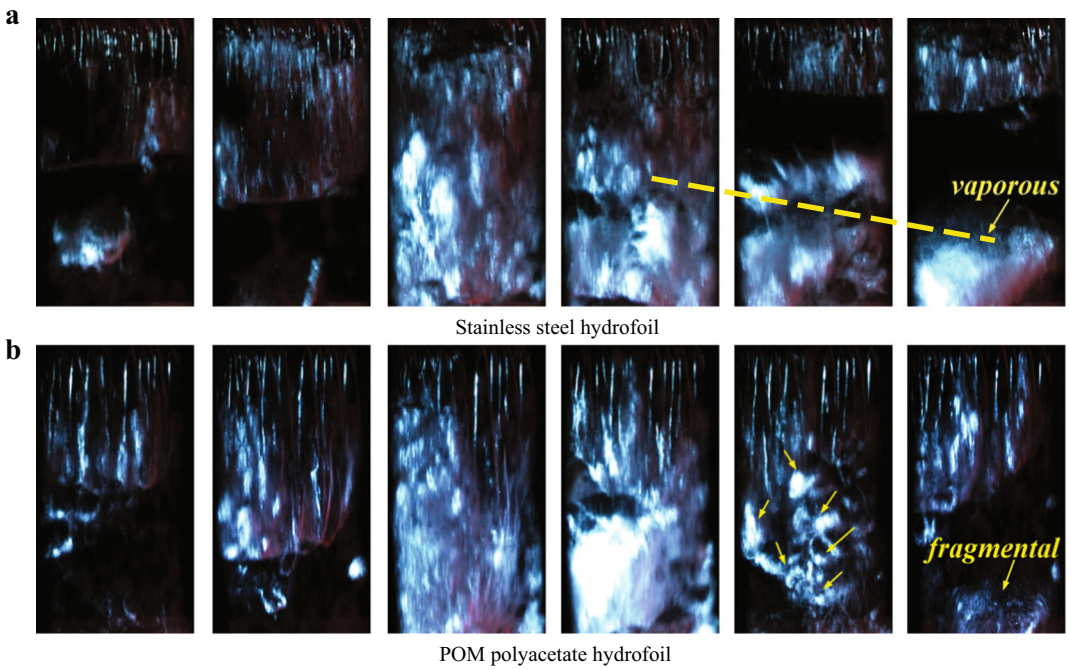

Fig. 24 Observations of the cavitation patterns for stainless steel and POM polyacetate hydrofoils

some experimental investigation has been addressed in the present paper, is it still urgently required to explore multi-field synchronized measurement methodology on the flow visualization, structural vibration, and deformation. Many advanced optical tools, such as high-speed 3D PIV and LDV, are being used for cavitating flow measurement. Meanwhile, pressure fluctuation has been considered as the main reason for the flow-induced vibrations, hence the synchronized accurate pressure measurement for rigid/flexible structures is necessary for the cavitation–structure interaction investigations.

As for the coupled fluid structure interaction model, more work is needed to improve the numerical results considering the unsteady response of the 3D elastic hydrofoil and the viscosity and turbulence of the transient cavitating flow.

7 Concluding remarks

In summary, recent progress on unsteady turbulent cavitating flow and corresponding flow-induced vibrations are reviewed in present work. A throughout survey of experimental and numerical methods for cavitation and cavitating flow-induced vibrations are presented to reveal the complicated transient flow mechanisms and cavitation–structure interactions. Meanwhile, the limitation of cavitating flow-induced vibration simulations and discrepancies between the numerical prediction and experimental measurement are still existed and more work is still needed.

In the present article, five topics are mainly involved.

(1) Global unsteady cavitating flow structures in different cavitation stages and corresponding flow-induced vibration characteristics are discussed. Among these, special focus has been given to the cloud cavitation and its synchronized structural vibrations. The trailing edge of the cloud cavity exhibits noticeable unsteady characteristics and significant interactions between the cavity and vortex structures, which leads to the large amplitude fluctuations of the structural vibration velocity.
(2) The numerical methods of cavitating turbulent flow and cavitation–structure interaction simulations are investigated. The ability of a transport cavitation model together with a suitable turbulence closure to predict the inception, growth, breakup, and shedding of the cavity is discussed. The proposed FBDCM approach reduces the turbulent eddy viscosity and can well capture the unsteady cavitation characteristics and dynamics. Various coupled fluid structure interaction models are discussed. Traditional coupled FSI algorithms tend to over-predict the structural displacement because they ignore the artificially added mass effect and the newly developed hybrid coupled algorithm is able to avoid numerical instability issued associated with it.
(3) Cavitation has a significant effect on the hydroelastic response, enhancing the bending and twisting deformation. Meanwhile, the hydroelastic response has affected the unsteady cavitation development and cavity-vortex interactions, with larger main cavity shedding frequency

and the vortex shedding frequency. The hydrodynamic load coefficients of the flexible hydrofoil fluctuate more significantly accompanied with the chaotic response, which is attributed to the structural flutter and deformations.

Acknowledgements The project was supported by the National Natural Science Foundation of China (Grant 51679005), the Natural Science Foundation of Beijing Municipality (Grant 3172029), and the Ph.D. Programs Foundation of Ministry of Education of China (Grant 20131101120014).

References

1. Brennen, C.E.: Cavitation and Bubble Dynamics. Oxford Engineering and Sciences Series, vol. 44. Oxford University Press, Oxford (1995)
2. Knapp, R.T., Daily, J.W., Hammitt, F.G.: Cavitation. McGraw Hill, New York (1970)
3. Ji, B., Wang, J., Luo, X., et al.: Numerical simulation of cavitation surge and vortical flows in a diffuser with swirling flow. J. Mech. Sci. Technol. **30**, 2507–2514 (2016)
4. Wang, Y., Wu, X., Huang, C., et al.: Unsteady characteristics of cloud cavitating flow near the free surface around an axisymmetric projectile. Int. J. Multiph. Flow **85**, 48–56 (2016)
5. Chen, Y., Chen, X., Li, J., et al.: Large Eddy Simulation and investigation on the flow structure of the cascading cavitation shedding regime around 3D twisted hydrofoil. Ocean Eng. **129**, 1–19 (2017)
6. Rood, E.P.: Review-mechanisms of cavitation inception. J. Fluids Eng. **113**, 163–175 (1991)
7. Kawanami, Y., Kato, H., Yamauchi, H., et al.: Mechanism and control of cloud cavitations. ASME J. Fluids Eng. **119**, 788–794 (1997)
8. Laberteaux, K.R., Ceccio, S.L.: Partial cavity flows. Part 1: Cavities forming on models without spanwise variation. ASME J. Fluid Mech. **431**, 1–41 (2002)
9. Delange, D.F., Debruin, G.J.: Sheet cavitation and cloud cavitation, re-entrant jet and three-dimensionality. Appl. Sci. Res. **58**, 91–114 (1997)
10. Kubota, A., Kato, H., Yamaguchi, H., et al.: Unsteady structure measurement of cloud cavitation on a foil section using conditional sampling technique. ASME J. Fluids Eng. **111**, 204–210 (1989)
11. Callenaere, M., Franc, J.P., Michel, J.M., et al.: The cavitation instability induced by the development of a re-entrant jet. ASME J. Fluid Mech. **444**, 233–256 (2001)
12. Kawakami, D.T., Fuji, A., Tsujimoto, Y., et al.: An assessment of the influence of cavitation instabilities. J. Fluids Eng. **130**, 1–8 (2008)
13. Li, C.Y., Ceccio, S.L.: Interaction of single travelling bubbles with the boundary layer and attached cavitation. J. Fluid Mech. **322**, 329–353 (1996)
14. Arndt, R.E.A., Song, C.C.S.: Instability of partial cavitation: a numerical/experimental approach. In: Proceedings of Twenty-Third Symposium on Naval Hydrodynamics, Valde Reuil, France (2000)
15. Li, X., Wang, G., Yu, Z., et al.: Multiphase fluid dynamics and transport processes of low capillary number cavitating flows. Acta. Mech. Sin. **25**, 161–172 (2009)
16. Ausoni, P., Farhat, M., Escaler, X., et al.: Cavitation influence on von Karman vortex shedding and induced hydrofoil vibrations. ASME J. Fluid Eng. **129**, 966–973 (2007)
17. Gopalan, S., Katz, J.: Flow structure and modeling issues in the closure region of attached cavitation. Phys. Fluids **12**, 895–911 (2000)
18. Dang, J., Kuiper, G.: Re-entrant jet modeling of partial cavity flow on three dimensional hydrofoils. ASME J. Fluids Eng. **121**, 781–787 (1999)
19. Dang, J.: Numerical simulation of unsteady partial cavity flows. [Ph.D. Thesis], Technical University of Delft, Netherlands (2000)
20. Foeth, E.J.: The structure of three-dimensional sheet cavitation. [Ph.D. Thesis], Delft University of Technology, Delft, Netherlands (2008)
21. Foeth, E.J., Van Terwisga, T., Van Doone, C.: On the collapse structure of an attached cavity on a three-dimensional hydrofoil. ASME J. Fluids Eng. **130**, 071303 (2008)
22. Tseng, C., Shyy, W.: Modeling for isothermal and cryogenic cavitation. Int. J. Heat Mass Trans. **53**, 513–525 (2010)
23. Leroux, J.-B., Astolfi, J.A., Billard, J.Y.: An experimental study of unsteady partial cavitation. J. Fluids Eng. **126**, 94–101 (2004)
24. Peng, X.X., Ji, B., Cao, Y.T., et al.: Combined experimental observation and numerical simulation of the cloud cavitation with U-type flow structures on hydrofoils. Int. J. Multiph. Flow **79**, 10–22 (2016)
25. Senocak, I., Shyy, W.: Evaluation of cavitation models for Navier–Stokes computations. In: Proceedings of FEDSM'02, ASME 2002 Fluids Engineering Division Summer Meeting Montreal, Quebec, Canada (2002)
26. Senocak, I., Shyy, W.: Interfacial dynamics-based modeling of turbulent cavitating flows. Part-1: Model development and steady-state computations. Int. J. Numer. Methods Fluids **44**, 975–995 (2004)
27. Senocak, I., Shyy, W.: Interfacial dynamics-based modeling of turbulent cavitating flows. Part-2: Time-dependent computations. Int. J. Numer. Methods Fluids **44**, 997–1016 (2004)
28. Kim, S., Brewton, S.: A multiphase approach to turbulent cavitating flows. In: Proceedings of 27th Symposium on Naval Hydrodynamics, Seoul, Korea (2008)
29. Zhao, Y., Wang, G., Huang, B.: A cavitation model for computations of unsteady cavitating flows. Acta. Mech. Sin. **32**, 1–11 (2016)
30. Hu, C., Wang, G., Chen, G., et al.: A modified PANS model for computations of unsteady turbulence for cavitating flows. Sci. China Phys. Mech. Astron. **57**, 1967–1976 (2014)
31. Chen, Y., Heister, S.D.: Modeling hydrodynamic non-equilibrium in cavitating flows. ASME J. Fluids Eng. **118**, 172–178 (1996)
32. Kubota, A., Kato, H., Yamaguchi, H.: A new modeling of cavitating flows: a numerical study of unsteady cavitation on a hydrofoil section. ASME J. Fluid Mech. **240**, 59–96 (1992)
33. Kunz, R.F., Boger, D.A., Stinebring, D.R., et al.: A preconditioned Navier–Stokes method for two phase flows with application to cavitation prediction. Comput. Fluids **29**, 849–875 (2000)
34. Singhal, A.K., Athavale, M.M., Li, H., et al.: Mathematical basis and validation of the full cavitation model. ASME J. Fluids Eng. **124**, 617–624 (2002)
35. Delannoy, Y., Kueny, J.L.: Two phase flow approach in unsteady cavitation modeling. In: Proceedings of the Spring Meeting of the Fluids Engineering Division, 153–158 (1990)
36. Wang, G., Ostoja-Starzewski, M.: Large eddy simulation of a sheet/cloud cavitation on a NACA0015 hydrofoil. Appl. Math. Model. **31**, 417–447 (2007)
37. Merkle, C.L., Feng, J., Buelow, P.E.O.: Computational modeling of sheet cavitations. In: Proceedings of Third International Symposium on Cavitation, Grenoble, France (1998)
38. Coutier-Delgosha, O., Fortes-Patella, R., Reboud, J.L.: Evaluation of the turbulence model influence on the numerical simulations of unsteady cavitations. ASME J. Fluids Eng. **125**, 38–45 (2003)

39. Kinzel, M.P., Lindau, J.W., Peltier, L.J., et al.: Detached-eddy simulations for cavitating flows. AIAA, 2007-4098 (2007)
40. Wu, J., Wang, G., Shyy, W.: Time-dependent turbulent cavitating flow computations with interfacial transport and filter based models. Int. J. Numer. Methods Fluids **49**, 739–761 (2005)
41. Reboud, J.L., Stutz, B., Coutier-Delgosha, O.: Two phase flow structure of cavitation: experiment and modeling of unsteady effects. In: Proceedings of the Third Symposium on Cavitation, Grenoble, France (1998)
42. Huang, B., Wang, G., Yu, Z., et al.: Detached-eddy simulation for time-dependent turbulent cavitating flows. Chin. J. Mech. Eng. **25**, 484–490 (2012)
43. Johansen, S.T., Wu, J., Shyy, W.: Filter-based unsteady RANS computations. Int. J. Heat Fluid Flow **25**, 10–21 (2004)
44. Song, M.T., Xu, L.H., Peng, X.X., et al.: An acoustic approach to determine tip vortex cavitation inception for an elliptical hydrofoil considering nuclei-seeding. Int. J. Multiph. Flow **90**, 79–87 (2017)
45. Arndt, R.E.A., Pennings, P., Bosschers, J., et al.: The singing vortex. Interface Focus **5**, 1–11 (2015)
46. Wang, Y.W., Liao, L.J., Du, T.Z., et al.: A study on the collapse of cavitation bubble surrounding the underwater-launched projectile and its fluid–structure coupling effects. Ocean Eng. **84**, 228–236 (2014)
47. Chae, E.J.: Dynamic Response and Stability of Flexible Hydrofoils in Incompressible and Viscous Flow. [Ph.D. Thesis], University of Michigan, Ann Arbor, America (2015)
48. Luo, X., Ji, B., Tsujimoto, Y.: A review of cavitation in hydraulic machinery. J. Hydrodyn. Ser. B **28**, 335–358 (2016)
49. Zobeiri, A., Ausoni, P., Avellan, F., et al.: How oblique trailing edge of a hydrofoil reduces the vortex-induced vibration. J. Fluids Struct. **32**, 78–89 (2012)
50. Ji, B., Luo, X.W., Arndt, R.E.A., et al.: Numerical simulation of three dimensional cavitation shedding dynamics with special emphasis on cavitation–vortex interaction. Ocean Eng. **87**, 64–77 (2014)
51. Chen, G., Wang, G., Hu, C., et al.: Combined experimental and computational investigation of cavitation evolution and excited pressure fluctuation in a convergent–divergent channel. Int. J. Multiph. Flow **72**, 133–140 (2015)
52. De La Torre, O., Escaler, X., Egusquiza, E., et al.: Experimental investigation of added mass effects on a hydrofoil under cavitation conditions. J. Fluids Struct. **39**, 173–187 (2013)
53. Amromin, E., Kovinskaya, S.: Vibration of cavitating elastic wing in a periodically perturbed flow: excitation of subharmonics. J. Fluids Struct. **14**, 735–751 (2000)
54. Kamakoti, R., Shyy, W.: Fluid–structure interaction for aeroelastic applications. Prog. Aerosp. Sci. **40**, 535–558 (2004)
55. Benaouicha, M., Astolfi, J.A., Ducoin, A.: A Numerical study of cavitation induced vibration. In: Proceedings of the ASME 2010 Pressure Vessels and Piping Division/K-PVP Conference. Bellevue, Washington, USA, 1–8 (2010)
56. Ryzhakov, P.B., Rossi, R., Idelsohn, S.R., et al.: A monolithic Lagrangian approach for fluid–structure interaction problems. Comput. Mech. **46**, 883–899 (2010)
57. Farhat, C., vander Zee, K., Geuzaine, Ph: Provably second-order time-accurate loosely-coupled solution algorithms for transient nonlinear aeroelasticity. Comput. Methods Appl. Mech. Eng. **195**, 1973–2001 (2006)
58. Campbell, R.L., Paterson, E.G.: Fluid–structure interaction analysis of flexible turbomachinery. J. Fluids Struct. **27**, 1376–1391 (2011)
59. Michler, C., Hulshoff, S.J., van Brummelen, E.H., et al.: A monolithic approach to fluid–structure interaction. Comput. Fluids **33**, 839–848 (2004)
60. Causin, P., Gerbeau, J.F., Nobile, F.: Added-mass effect in the design of partitioned algorithms for fluid–structure problems. Comput. Methods Appl. Mech. Eng. **194**, 4506–4527 (2005)
61. Young, Y.L., Chae, E.J., Akcabay, D.T.: Hybrid algorithm for modeling of fluid–structure interaction in incompressible viscous flows. Acta Mech. Sin. **28**, 1030–1041 (2012)
62. Matthies, H.G., Steindorf, H.: Partitioned strong coupling algorithms for fluid–structure interaction. Comput. Struct. **81**, 805–812 (2003)
63. Belanger, F., Paidoussis, M.P., Langre, E.: Time-marching analysis of fluid-coupled systems with large added mass. AIAA J. **33**, 752–757 (1995)
64. Forster, C., Wall, W.A., Ramm, E.: Artificial added mass instabilities in sequential staggered coupling of nonlinear structures and incompressible viscous flows. Comput. Methods Appl. Mech. Eng. **196**, 1278–1293 (2007)
65. Grekula, M., Bark, G.: Experimental study of cavitation in a Kaplan model turbine. In: Proceedings of 4th International Symposium on Cavitation, Pasadena, Ca, USA (2001)
66. Sato, K., Shimojo, S.: Detailed observations on a starting mechanism for shedding of cavitation cloud. In: Proceedings of 5th International Symposium on Cavitations, Japan (2003)
67. Amromin, E.: Development and validation of CFD models for initial stages of cavitation. J. Fluids Eng. **136**, 1–33 (2014)
68. Arakeri, V.H., Acosta, A.J.: Viscous effects in the inception of cavitation on axisymmetric bodies. ASME J. Fluid Eng. **95**, 519–527 (1973)
69. Foeth, E.J., Van Doorne, C.W.H., Van Terwisga, T., et al.: Time resolved PIV and flow visualization of 3D sheet cavitation. Exp. Fluids **40**, 503–513 (2006)
70. Stutz, B., Reboud, J.L.: Two-phase flow structure of sheet cavitations. Phys. Fluids **9**, 3678–3686 (1997)
71. Ji, B., Luo, X., Wu, Y., et al.: Partially-averaged Navier–Stokes method with modified k-e model for cavitating flow around a marine propeller in a non-uniform wake. Int. J. Heat Mass Transf. **55**, 6582–6588 (2012)
72. Stutz, B., Reboud, J.L.: Experiments on unsteady cavitation. Exp. Fluids **22**, 191–198 (1997)
73. Li, X., Wang, G., Zhang, M., et al.: Structures of supercavitating multiphase flows. Int. J. Therm. Sci. **47**, 1263–1275 (2008)
74. Long, X., Zhang, J., Wang, Q., et al.: Experimental investigation on the performance of jet pump cavitation reactor at different area ratios. Exp. Therm. Fluid Sci. **78**, 309–321 (2016)
75. Fukaya, M., Ono, S., Udo, R.: Prediction of cavitation intensity in pumps based on propagation analysis of bubble collapse pressure using multi-point vibration acceleration method. Int. J. Fluid Mach. Syst. **2**, 165–171 (2009)
76. Ducoin, A., Astolfi, J.A., Gobert, M.-L.: An experimental study of boundary-layer transition induced vibrations on a hydrofoil. J. Fluids Struct. **32**, 37–51 (2012)
77. Wu, Q., Huang, B., Wang, G.: Experimental and numerical investigation of hydroelastic response of a flexible hydrofoil in cavitating flow. Int. J. Multiph. Flow **74**, 19–33 (2015)
78. Leroux, J.B., Coutier-Delgosha, O., Astolfi, J.A.: A joint experimental and numerical study of mechanisms associated to instability of partial cavitation on two-dimensional hydrofoil. Phys. Fluids **17**, 1–20 (2005)
79. Akcabay, D.T., Chae, E.J., Young, Y.L., et al.: Cavity induced vibration of flexible hydrofoils. J. Fluids Struct. **49**, 463–484 (2014)
80. Zhang, B.: Physical and numerical investigation of unsteady cavitating flow mechanism and hydrodynamic characteristics. [Ph.D. Thesis], Beijing Institute of Technology, China (2009)
81. Luo, X.W., Ji, B., Zhang, Y., et al.: Cavitating flow over a mini hydrofoil. Chin. Phys. Lett. **29**, 016401 (2012)

82. Dular, M., Khlifa, I., Fuzier, S., et al.: Scale effect on unsteady cloud cavitation. Exp. Fluids **53**, 1233–1250 (2012)
83. Wang, G., Liu, S., Shintani, M., et al.: Study on cavitation damage characteristics around a hollow-jet valve. JSME Int. J. Ser. B **42**, 649–658 (1999)
84. Wang, G.Y., Senocak, I., Shyy, W., et al.: Dynamics of attached turbulent cavitating flows. Prog. Aerosp. Sci. **37**, 551–581 (2001)
85. Kim, D.J., Sung, H.J., Choi, C.H., et al.: Cavitation instabilities of an inducer in a cryogenic pump. Acta Astronaut. **132**, 19–24 (2017)
86. Ji, B., Luo, X.W., Wu, Y.L., et al.: Numerical and experimental study on unsteady shedding of partial cavitation. Mod. Phys. Lett. B **24**, 1441–1444 (2010)
87. Huang, B., Wang, G.: Experimental and numerical investigation of unsteady cavitating flows through a 2D hydrofoil. Sci. China Tech. Sci. **54**, 1801–1812 (2011)
88. Peng, X.X., Ji, B., Cao, Y., et al.: Combined experimental observation and numerical simulation of the cloud cavitation with U-type flow structures on hydrofoils. Int. J. Multiph. Flow **79**, 10–22 (2016)
89. Wu, Q., Wang, G.Y., Huang, B., et al.: Experimental investigation of the flow-induced vibration of hydrofoils in cavitating flows. J. Phys. Conf. Ser. **656**, 012105 (2015)
90. Huang, B., Young, Y.L., Wang, G.Y., et al.: Combined experimental and computational investigation of unsteady structure of sheet/cloud cavitation. J. Fluids Eng. **135**, 071301 (2013)
91. Kato, H., Konno, A., Maeda, M., et al.: Possibility of quantitative prediction of cavitation erosion without model test. ASME J. Fluids Eng. **118**, 582–588 (1996)
92. Kirschner, I.N., Fine, N.E., Uhlman, J.S., et al.: Numerical modeling of supercavitating flows. Technical report. DTIC (2001)
93. Semenenko, V.N.: Artificial supercavitation: physics and calculation. RTO AVT/VKI special course: supercavitating flows, von Karman Institute for Fluid Dynamics, Rhode-Saint-Genese, Belgium, 12–16 (2001)
94. Shen, Y., Dimotakis, P.: The influence of surface cavitation on hydrodynamic forces. In: Proceedings of 22nd ATTC, St. Johns, 44–53 (1989)
95. Ducoin, A., Huang, B., Young, Y. L.: Y.L.: Numerical modeling of unsteady cavitating flows around a stationary hydrofoil. Int. J. Rotating Mach. Mach. 2012, 215678, 1–17 (2012)
96. Luo, X.W., Ji, B., Peng, X.X., et al.: Numerical simulation of cavity shedding from a three-dimensional twisted hydrofoil and induced pressure fluctuation by large-eddy simulation. ASME J. Fluids Eng. Trans. **134**, 041202 (2012)
97. Zwart, P., Gerber, A., Belamri, T.: A two-phase flow model for predicting cavitation dynamics. In: Fifth International Conference on Multiphase Flow, Yokohama, Japan (2004)
98. Ducoin, A., Huang, B., Young, Y.L.: Numerical modeling of unsteady cavitating flows around a stationary hydrofoil. Int. J. Rotating Mach. Article **2012**, (2012)
99. Huang, B.,Ducoin, A.,Young,Y.L.:Evaluation of cavitation models for prediction of transient cavitating flows around a pitching hydrofoil. In: Proceedings of 8th International Symposium on Cavitation, Singapore (2012)
100. Launder, B.E., Spalding, D.B.: The numerical computation of turbulent flows. Comput. Methods Appl. Mech. Eng. **3**, 269–289 (1974)
101. Cho, Y.C., Du, W., Gupta, A., et al.: Surrogate-based modeling and dimension-reduction techniques for thermo-fluid and energy systems. In: Proceeding of the ASME/JSME 2011 8th Thermal Engineering Joint Conference, Honolulu, Hawaii, USA, March 13–17 (2011)
102. Hu, C., Wang, G., Chen, G., et al.: Surrogate model-based optimization for the headform design of an axisymmetric body. Ocean Eng. **107**, 237–245 (2015)
103. Shyy, W., Cho, Y.-C., Du, W., et al.: Surrogate-based modeling and dimension reduction techniques for multi-scale mechanics problems. Acta. Mech. Sin. **27**, 845–865 (2011)
104. Wu, Q., Wang, G.Y., Huang, B.: Parameter optimization and analysis of a filter-based density correction model. J. Ship Mech. **20**, 789–798 (2016)
105. Crank, J., Nicolson, P.: A practical method for numerical evaluation of solutions of partial differential equations of the heat-conduction type. Adv. Comput. Math. **6**, 207–226 (1996)
106. Klostermann, J., Schaake, K., Schwarze, R.: Numerical simulation of a rising bubble by VOF with surface compression. Int. J. Numer. Methods Fluids **71**, 960–982 (2013)
107. Theodorsen, T.: General theory of aerodynamic instability and the mechanism of flutter. National Advisory Committee for Aeronautics, Technical Report, No. 496 (1935)
108. Ducoin, A., Young, Y.L.: Hydroelastic response and stability of a hydrofoil in viscous flow. J. Fluids Struct. **38**, 40–57 (2013)
109. Huang, B., Zhao, Y., Wang, G.: Large eddy simulation of turbulent vortex–cavitation interactions in transient sheet/cloud cavitating flows. Comput. Fluids **92**, 113–124 (2014)
110. Young, Y.L., Motley, M.R., Yeung, R.W.: Three-dimensional numerical modeling of the transient fluid–structural interaction response of tidal turbines. J. Offshore Mech. Arctic Eng. **132**, 011101 (2010)
111. Stenius, I., Rosen, A., Kuttenkeuler, J.: Hydroelastic interaction in panel-water impacts of high speed craft. Ocean Eng. **38**, 371–381 (2011)
112. Chimakurthi, S.K., Tang, J., Palacios, R., et al.: Computational aeroelasticity framework for analyzing flapping wing micro air vehicles. AIAA J. **47**, 1865–1878 (2009)
113. Ducoin, A.: Etude experimentale et numerique du chargement hydrodynamique des corps portants en regime transitoire avec prise en compte du couplage fluide structure. [Ph.D. Thesis], Ecole Centrale de Nantes, France (2008) (in French)